Received: 30 January 2023 | Revised: 15 November 2023 | Accepted: 23 November 2023

DOI: 10.1002/jev2.12394

RESEARCH ARTICLE

Extracellular vesicle-associated cholesterol supports the regenerative functions of macrophages in the brain

Sam Vanherle[1,2] | **Jeroen Guns**[1,2] | **Melanie Loix**[1,2] | **Fleur Mingneau**[1,2] | **Tess Dierckx**[1,2] | **Flore Wouters**[1,2] | **Koen Kuipers**[1,2] | **Tim Vangansewinkel**[3,4] | **Esther Wolfs**[3] | **Paula Pincela Lins**[3,5] | **Annelies Bronckaers**[3] | **Ivo Lambrichts**[3] | **Jonas Dehairs**[6] | **Johannes V. Swinnen**[6] | **Sanne G. S. Verberk**[1,2] | **Mansour Haidar**[1,2] | **Jerome J. A. Hendriks**[1,2] | **Jeroen F. J. Bogie**[1,2]

[1]Department of Immunology and Infection, Biomedical Research Institute, Hasselt University, Diepenbeek, Belgium

[2]University MS Center Hasselt, Pelt, Belgium

[3]Department of Cardio and Organs Systems, Biomedical Research Institute, Hasselt University, Diepenbeek, Belgium

[4]VIB, Center for Brain & Disease Research, Laboratory of Neurobiology, University of Leuven, Leuven, Belgium

[5]Health Department, Flemish Institute for Technological Research, Mol, Belgium

[6]Department of Oncology, Laboratory of Lipid Metabolism and Cancer, Leuven Cancer Institute, University of Leuven, Leuven, Belgium

Correspondence
Jeroen F. J. Bogie, Department of Immunology and Infection, Biomedical Research Institute, Hasselt University, Diepenbeek, Agoralaan gebouw C, 3590 Diepenbeek, Belgium. Email: jeroen.bogie@uhasselt.be

Funding information
Fonds Wetenschappelijk Onderzoek, Grant/Award Numbers: 1141920N, 11M1722N, 12J9119N, 1S15519N, G099618FWO; Interreg Vlaanderen-Nederland, Grant/Award Numbers: EURLIPIDS, EMR23

Abstract

Macrophages play major roles in the pathophysiology of various neurological disorders, being involved in seemingly opposing processes such as lesion progression and resolution. Yet, the molecular mechanisms that drive their harmful and benign effector functions remain poorly understood. Here, we demonstrate that extracellular vesicles (EVs) secreted by repair-associated macrophages (RAMs) enhance remyelination ex vivo and in vivo by promoting the differentiation of oligodendrocyte precursor cells (OPCs). Guided by lipidomic analysis and applying cholesterol depletion and enrichment strategies, we find that EVs released by RAMs show markedly elevated cholesterol levels and that cholesterol abundance controls their reparative impact on OPC maturation and remyelination. Mechanistically, EV-associated cholesterol was found to promote OPC differentiation predominantly through direct membrane fusion. Collectively, our findings highlight that EVs are essential for cholesterol trafficking in the brain and that changes in cholesterol abundance support the reparative impact of EVs released by macrophages in the brain, potentially having broad implications for therapeutic strategies aimed at promoting repair in neurodegenerative disorders.

KEYWORDS
cholesterol, extracellular vesicle, oligodendrocyte precursor cell differentiation, remyelination, repair-associated macrophage

1 | INTRODUCTION

Chronic demyelinating diseases of the central nervous system (CNS) are characterized by loss of the protective myelin sheath, leaving axons and even complete neurons vulnerable to degeneration (Franklin & Ffrench-Constant, 2017). In early disease stages, endogenous repair processes are apparent, evidenced by lesional migration of oligodendrocyte progenitor cells (OPCs) and their

Jerome J. A. Hendriks and Jeroen F. J. Bogie contributed equally to this study.

successive differentiation into mature myelinating oligodendrocytes (OLNs) (Di Bello et al., 1999; Fancy et al., 2010; Franklin & Ffrench-Constant, 2017). However, as the disease progresses, endogenous repair mechanisms frequently fail, resulting in the formation of chronically demyelinated lesions and widespread axonal and neuronal degeneration (Cantuti-Castelvetri et al., 2018; Hagemeier et al., 2012; Hanafy & Sloane, 2011; Wolswijk, 2002). These cytodegenerative events are anticipated to drive clinical deterioration in patients, often leading to irreversible physical, neurological and cognitive incapacitation. Emerging evidence indicates that failure of remyelination relies on microenvironmental factors to which OPCs are exposed to in demyelinating lesions (Neumann et al., 2019; Wang et al., 2020; Woodruff et al., 2004). To date, however, the cell types, soluble factors and molecular mechanisms involved remain poorly understood.

Dysfunction or imbalances in the macrophage phenotype are increasingly being acknowledged to drive demyelinating events and underlie failure of remyelination in the CNS (Bogie et al., 2020; Cantuti-Castelvetri et al., 2018; Kotter et al., 2001, 2005; Marschallinger et al., 2020; McNamara et al., 2022; Miron et al., 2013; Sariol et al., 2020; Vanherle et al., 2022). In support of this notion, CNS lesions are characterized by abundant accumulation of disease-associated macrophages (DAMs), which are considered to promote demyelination and hamper remyelination through the release of inflammatory and toxic mediators that negatively impact OPCs, OLNs and neuronal homeostasis (Bogie et al., 2020; Cantuti-Castelvetri et al., 2018; Marschallinger et al., 2020; McMahon et al., 2002; Nikić et al., 2011; Trapp et al., 1998). Whereas macrophages can acquire disease-resolving features, including the release of neurotrophic factors and clearance of inhibitory myelin debris (Bogie et al., 2020; Miron et al., 2013; Ruckh et al., 2012), the induction of such repair-associated macrophages (RAMs) appears to be transient. Accordingly, we and others demonstrated that, in time, perturbed lipid metabolism quenches and promotes the formation of RAMs and DAMs, respectively (Bogie et al., 2020; Cantuti-Castelvetri et al., 2018). Despite being closely associated with lesion progression and resolution, the harmful and benign effector mechanisms of RAMs and DAMs are ill-defined. Identifying factors that underlie the effector functions of RAMs and DAMs is essential for our understanding of lesion progression in chronic demyelinating disorders and the development of pro-regenerative therapies.

Extracellular vesicles (EVs) are nanosized particles surrounded by a lipid bilayer membrane that transport biologically active molecules such as proteins, nucleic acids and lipids from donor cells to distant and neighbouring recipient cells, thereby affecting recipient cell physiology (Kalluri & LeBleu, 2020; Vanherle et al., 2020). Emerging evidence indicates that EVs are associated with degenerative and regenerative events in the CNS (Guo et al., 2020; Herman et al., 2022; Hervera et al., 2018), and that modified EVs represent a promising therapeutic tool to promote CNS repair (Cooper et al., 2014; Wang et al., 2019; Zhang et al., 2021). Here, we report that EVs released by RAMs enhance OPC maturation in vitro, and promote myelin regeneration in ex vivo and in vivo models that mimic remyelination. Guided by lipidomic analysis, we find that the pro-regenerative impact of EVs released by RAMs is ascribed to increased cholesterol abundance in these EVs. Accordingly, the enrichment of cholesterol in EVs released by DAMs markedly enhances their regenerative properties. Finally, we provide evidence that direct membrane incorporation of EV-associated cholesterol via membrane fusion partially underlies the regenerative impact of EVs released by RAMs on OPC maturation and remyelination. Collectively, our findings highlight that EVs are essential for cholesterol trafficking and that changes in cholesterol abundance contribute to the benign impact of EVs released by macrophages in the CNS.

2 | MATERIALS AND METHODS

2.1 | Antibodies and chemical reagents

The following antibodies were used for immunofluorescent/immunohistochemical stains: anti-Flotillin 1 (1:1000, cat. #D2V7J, Cell Signalling Technology), anti-CD81 (1:1000, cat. #D502Q, Cell Signalling Technology), anti-Annexin A2 (1:1000, cat. #D1162, Cell Signalling Technology), anti-GRP94 (1:1000, cat. #D6 × 2Q, Cell Signalling Technology), anti-MBP (1:250 (in vivo, ex vivo) or 1:500 (in vitro), cat. #MAB386, Millipore), anti-O4 (1:1000, cat. #MAB1326, R&D systems), anti-Olig2 (1:100, cat. #AF2418, R&D systems), anti-CC1 (1:100, cat. #ab16794, Sigma-Aldrich), anti-NF (1:1000, cat. #ab8135, Sigma-Aldrich). Appropriate secondary antibodies were purchased from Invitrogen. Methyl-β-cyclodextrin (MβCD; 1, 2.5, or 5 mg/mL, cat. #C4555, Sigma-Aldrich) was used to deplete EVs from cholesterol or was complexed with cholesterol (7.3 mM, cat. #C3045, Sigma-Aldrich) to enrich EVs with cholesterol. GW4869 (10 μM, cat. #HY-19363, MedChemExpress) was used to inhibit EV biogenesis. Cytochalasin D (10 μM, cat. #C8273, Sigma-Aldrich), chlorpromazine hydrochloride (50 μM, cat. #C8138, Sigma-Aldrich), nystatin (25 μM, cat. #N4014, Sigma-Aldrich), imipramine hydrochloride (5 μM, cat. #I7379, Sigma-Aldrich), wortmannin (500 nM, cat. #W1628, Sigma-Aldrich), omeprazole (50 μM, cat. #O104, Sigma-Aldrich) and MβCD (2 mg/mL, cat. #C4555, Sigma-Aldrich) were used to inhibit specific EV uptake pathways. T0901317 (10 μM, cat. #71810, Cayman Chemicals) was used as LXR agonist.

2.2 | Animals

Wild-type C57BL/6J mice were purchased from Envigo and were housed in a 12 h light/dark cycle with ad libitum access to water and a standard chow diet or specific formulations as indicated. All animal procedures were conducted in accordance with the

institutional guidelines and approved by the Ethical Committee for Animal Experiments of Hasselt University (protocol numbers 201802, 201934K, 201967).

2.3 | EV production and isolation

Bone marrow-derived macrophages (BMDMs) were obtained as described previously (Bogie et al., 2017). Briefly, femoral and tibial bone marrow was isolated from 11-week-old female wild-type C57BL/6J mice and cultured in 14.5 cm petri dishes (Greiner, ref. 639161) at a concentration of 10×10^6 cells/petri dish in RPMI1640 medium (Lonza) supplemented with 10% fetal calf serum (FCS; Biowest), 50 U/mL penicillin (Invitrogen), 50 U/mL streptomycin (Invitrogen), and 15% L929-conditioned medium (LCM) for 7 days at 37°C and 5% CO_2. Next, cells were cultured at a density of 0.5×10^6 cells/mL in RPMI1640 supplemented with 10% FCS, 50 U/mL penicillin, 50 U/mL streptomycin, and 5% LCM at a total of 13.5×10^6 cells in T175 culture flasks (Greiner). Subsequently, BMDMs were treated for 6 h with vehicle, LPS (100 ng/μL, Sigma-Aldrich), or IL-4 (20 ng/μL, Peprotech) to induce naive macrophages (M0), DAMs or RAMs, respectively, after which BMDMs were cultured in complete medium. The next morning, conditioned medium was collected, shortly centrifuged to remove detached cells, and stored at −80°C. Astrocytes were isolated as described previously (Bogie et al., 2020). Briefly, astrocytes are obtained from P0-2 wild-type C57BL/6J mice cerebral cortices, and cells were enzymatically dissociated for 20 min at 37°C with papain (3 U/mL, Sigma-Aldrich), diluted in Dulbecco's Modified Eagle Medium (DMEM; Gibco) and supplemented with 1 mM L-cysteine (Sigma-Aldrich), and DNase I (20 μg/mL, Sigma-Aldrich). The resulting mixed glial cells were cultured in DMEM supplemented with 10% FCS, 50 U/mL penicillin, and 50 U/mL streptomycin in poly-L-lysine (PLL; 50 μg/mL, Sigma-Aldrich)-coated T75 culture flasks at 37°C and 8.5% CO_2. After 2 weeks of cultivation, cultures were shaken for 16 h at 250 rpm and 37°C. After shake-off, mixed glial cultures were cultured at a density of 0.5×10^6 cells/mL in DMEM supplemented with 10% FCS, 50 U/mL penicillin, and 50 U/mL streptomycin, at a total of 13.5×10^6 cells in T175 culture flasks. Peripheral blood mononuclear cells (PBMCs) were obtained from healthy donors and age- and gender-matched relapse-remitting MS patients (untreated) using density gradient centrifugation. PBMCs were cultured at a density of 0.5×10^6 cells/mL in RPMI1640 medium supplemented with 10% human serum, 1% sodium pyruvate (Sigma-Aldrich), 1% non-essential amino acid (NEAA; Sigma-Aldrich), 50 U/mL penicillin, and 50 U/mL streptomycin, at a total of 13.5×10^6 cells in T175 culture flasks. Next, BMDMs, astrocyte and PBMCs were cultured in EV-depleted culture medium (culture medium centrifuged for 16 h at 115,000 *g*, followed by 0.2 μm filtration) and medium was collected after 1 h (repeated four times). Thereafter, EVs were pelleted using a differential centrifugation method. Briefly, the collected supernatant was consecutively centrifuged at 300 *g* for 10 min, 2000 *g* for 10 min, and 10,000 *g* for 30 min, all at 4°C. Subsequently, the supernatant was centrifuged for 3 h at 115,000 *g* and 4°C using the XPN-80 ultracentrifuge equipped with a Ti70 rotor (Beckman). EV pellets were resolved in 1 mL ice-cold PBS (Gibco) and further purified by means of size exclusion chromatography (SEC) using a chromatography column (Bio-Rad Laboratories) filled with 10 mL Sepharose CL-2B beads (GE Healthcare). Sequential fraction 3.5 until 5.5 mL was collected from the flow-through and further concentrated using the Amicon Ultra 0.5 mL 10 kDa filter (Millipore). To isolate EV-associated lipids, EVs were destroyed by hypo-osmotic shock and pelleted as previously described (Gabrielli et al., 2015). Lipids were extracted using chloroform and methanol (2:1 v/v), and subsequently, the lipid fraction was evaporated and dried for 1 h at 50°C. Next, EV-associated lipids were resuspended in PBS at 40°C and sonicated to obtain small vesicles.

2.4 | Nanoparticle tracking analysis

To determine the size and concentration of BMDM-derived EVs, Nanoparticle Tracking Analysis (NTA) was performed using the NanoSight NS300 system (Malvern Panalytical), equipped with a 532 nm laser. Samples were diluted in PBS over a concentration range between 20 and 50 particles per frame. All settings were manually set at the start of the measurements and maintained during all acquisitions: camera level 14, camera gain 1, pump rate 80, viscosity 1. A minimum of three recordings of 30 s was recorded and analysed using the NTA software 3.0 with default settings.

2.5 | Western blot

EVs were lysed in ice-cold Radio-Immunoprecipiration Assay (RIPA) buffer (150 mM NaCl, 50 mM Tris, 1% SDS, 1% Triton X-100, and 0.5% sodium deoxycholate) supplemented with protease-phosphatase inhibitor cocktail (Roche). Pierce BCA Protein Assay kit (Thermo Fisher Scientific) was used to determine protein concentration, according to the manufacturer's guidelines. Samples were separated by electrophoresis on a 10% SDS-PAGE gel and were transferred onto a PVDF membrane. Blots were blocked using 5% dried skimmed milk powder (Marvel) in 1x PBS-0.1% Tween-20 (PBS-T), incubated overnight with the relevant primary antibody, followed by incubation with the appropriate HRP-conjugated secondary antibody. Chemiluminescent signals

were detected with the Amersham Imager 680 (GE Healthcare Life Sciences), using the enhanced chemiluminescence (ECL) Plus detection kit (Thermo Fisher Scientific).

2.6 | Cuprizone-induced acute demyelination in vivo model

To induce acute demyelination, 9-week-old male wild-type C57BL/6J mice were fed a diet containing 0.3% (w/w) cuprizone (bis[cyclohexanone]oxaldihydrazone, Sigma-Aldrich) mixed in powdered standard chow ad libitum for 5 weeks. Mice were subsequently subjected to a stereotactic injection of either vehicle or BMDM-derived EVs. Briefly, mice were anesthetized by intraperitoneal injection with a mixture of 10% w/v ketamine (Anesketin, Dechra), 2% w/v xylazine (Rompun, Bayer), and PBS (1 mg ketamine and 0.12 mg xylazine per 10 g body weight, dose volume 0.1 mL/10 g). Next, vehicle or BMDM-derived EVs (1×10^9 EVs) were unilaterally (left hemisphere) injected (AP 1.1 mm, ML −0.7 mm, DV −2.0 mm, relative to bregma) using a 10 μL Hamilton syringe at a speed of 1 μL/min. After injection, the needle was kept in place for an additional 2 min. After treatment, cuprizone diet was withdrawn to allow spontaneous remyelination. To define the effect of peripheral treatment, vehicle or BMDM-derived EVs (5×10^9 EVs) were daily administrated intranasally. 5 or 6 weeks after the start of cuprizone diet, mice were sacrificed and tissue was collected for histological and biochemical analysis.

2.7 | Cerebellar brain slice cultures

Cerebellar brain slices were obtained from wild-type C57BL/6J mouse pups at postnatal day 10 (P10), as described previously (Hussain et al., 2011; Meffre et al., 2015). Brain slices were cultured in MEM medium (Thermo Fisher Scientific) supplemented with 25% horse serum (Thermo Fisher Scientific), 25% Hank's balanced salt solution (Sigma-Aldrich), 50 U/mL penicillin, 50 U/mL streptomycin, 1% Glutamax (Thermo Fisher Scientific), 12.5 mM HEPES (Thermo Fisher Scientific) and 1.45 g/L glucose (Sigma-Aldrich). For BMDM replenishment experiments, phagocytes were depleted by treating slices with clodronate or empty liposomes (0.5 mg/mL, LIPOSOMA) immediately after isolation for 24 h. Next, slices were repleted with 4×10^3 LPS- or IL-4-stimulated BMDMs, which were either treated with vehicle or GW4869 (10 μM) to inhibit EV biogenesis. The BMDMs were added directly to the slice in a 1.5 μL drop, without touching the slice. Next, slices were left to recover for 2 days. To induce demyelination, brain slices were treated with 0.5 mg/mL lysolecithin (Sigma-Aldrich) at 3 days post isolation for 16 h. Next, brain slices were allowed to recover in culture medium for 1 day and subsequently treated daily with vehicle, BMDM-derived EVs, astrocyte-derived EVs (2×10^9 EVs/mL), empty liposomes or GW4869 liposomes (in house production) for 1 week, followed by histological and biochemical analysis.

2.8 | Liposome preparation

To prepare liposomes, 8 mg of cholesterol was dissolved in 10 mL of chloroform. Phosphatidylcholine (86 mg, cat. #Y0001905, Sigma-Aldrich) was added, and the solution was kept under a nitrogen stream for 5–10 min. Next, the resulting lipid film was dissolved in PBS with or without GW4869 (4.3 μM), followed by gentle shaking to obtain multilamellar vesicles (MLVs). Subsequently, MLVs were ultrasonicated for 3 min to obtain liposomes. Finally, the solution was centrifuged at 10.000 *g* to remove unencapsulated GW4869.

2.9 | OPC isolation and differentiation

OPCs were isolated as described previously (Dierckx et al., 2022). Briefly, OPCs were obtained from P0-2 wild-type C57BL/6J mice cerebral cortices, and cells were enzymatically dissociated for 20 min at 37°C with papain (3 U/mL, Sigma-Aldrich), diluted in DMEM and supplemented with 1 mM L-cysteine, and 20 μg/mL DNase I. The resulting mixed glial cells were cultured in DMEM supplemented with 10% FCS, 50 U/mL penicillin, and 50 U/mL streptomycin in PLL (50 μg/mL)-coated T75 culture flasks at 37°C and 8.5% CO_2. Medium change was performed on day 4, 7 and 11, and from day 7, cultures were supplemented with bovine insulin (5 μg/mL, Sigma-Aldrich). On day 14, OPCs were isolated using the orbital shake-off method. Briefly, cultures were first shaken at 75 rpm and 37°C for 45 min to detach microglia, and next, cultures were shaken for 16 h at 250 rpm and 37°C to detach OPCs. Subsequently, OPC-containing supernatant was incubated on a Petri dish for 20 min at 37°C and centrifuged at 300 *g*. Afterward, OPCs were plated on PLL-coated wells at a density of 3×10^5 cells/mL in proliferation medium (DMEM medium supplemented with 0.3 mM transferrin, 0.1 mM putrescin, 0.02 mM progesterone, 0.2 μM sodium selenite, 0.5 μM triiodothyronine, 0.5 mM L-thyroxin, 0.8 mM bovine insulin, 50 U/mL penicillin, 50 U/mL streptomycin, 2% horse serum, 2% B27 supplement, 5 ng/μL platelet-derived growth factor α (PDGFα) and 5 ng/μL fibroblast growth factor (FGF); all from

Sigma-Aldrich except for penicillin/streptomycin (Invitrogen), B27 (in house production as described by Chen et al.), and PDGFα/FGF (Peprotech) for 2 days. Next, OPCs were cultured in differentiation medium (proliferation medium without PDGFα/FGF) and treated daily for 6 days with vehicle, conditioned medium, or BMDM-derived EVs (4×10^8 EVs/mL).

2.10 | Transmission electron microscopy

EVs were negatively stained by 2% uranyl acetate. Briefly, 10 µL of EVs at an average concentration of 10^{11} EVs/mL were drop-casted on copper grids (TEDPELLA, #01824) for 60 s and dried with filter paper. Next, samples were stained by two steps of 3 µL 2% uranyl acetate for 30 s. Mouse brain samples were fixed with 2% glutaraldehyde. Next, post-fixation was done with 2% osmiumtetroxide in 0.05 M sodium cacodylate buffer for 1 h at 4°C. Dehydration of the samples was performed by ascending concentrations of acetone. Next, the dehydrated samples were impregnated overnight in a 1:1 mixture of acetone and araldite epoxy resin. Next, the samples were embedded in araldite epoxy resin at 60°C and were cut in slices of 70 nm, perpendicular to the corpus callosum, with a Leica EM UC6 microtome. The slices were transferred to copper grids (Veco B.V) that were coated with 0.7% formvar. Analysis was performed with a Jeol JEM-1400 Flash at 80 kV equipped with an Emsis 20 NP XAROSA camera system; for the EV images were collected images in at least 10 different grid regions and for the mouse brain sections around 5–12 images were taken. ImageJ was used to calculate the g-ratio (ratio of the inner axonal diameter to the total outer diameter). All analyses were conducted by observers blinded to the experimental arm of the study.

2.11 | Immunofluorescence

Murine OPCs were cultured on PLL-coated glass cover slides and fixed in 4% paraformaldehyde (PFA) for 20 min at room temperature. Cerebellar brain slices were fixed in 4% PFA for 15 min at room temperature. Brain tissue of cuprizone mice was isolated, snap-frozen, and sectioned with a Leica CM1900UV cryostat (Leica Microsystems) to obtain 10 µm slices. Cryosections were fixed in ice-cold acetone for 10 min at −20°C. Immunostaining and analysis of cryosections were performed as described previously (Bogie et al., 2017). ImageJ was used to align the corpus callosum (coronal section between bregma 0 and −0.5 mm), followed by determination of the MBP, Olig2 and CC1 positive signal in this area. To stain OPCs, samples were incubated with the relevant primary antibodies diluted in blocking buffer (1x PBS + 1% BSA + 0.1% Tween-20). To stain cerebellar brain slices, samples were incubated with relevant primary antibodies diluted in blocking buffer (1x PBS + 5% horse serum + 0.3% Triton X-100). Analysis of OPCs and cerebellar brain slices was performed using the LeicaDM2000 LED fluorescence microscope and the LSM 880 confocal microscope (Zeiss), respectively. ImageJ was used to determine the MBP/O4 positive area per cell and to define the Sholl analysis parameters related to process complexity and branching (sum intersections, average intersections/Sholl ring, end radius) in OPCs as previously described (Murtie et al., 2007), and to define the Olig2 and CC1 positive cells in the cerebellar brain slices, which is presented as the percentage $Olig2^+$ $CC1^+$ cells/$CC1^+$ cells, and the myelination index (MBP^+ NF^+ axons/NF^+ axons) which is presented in a relative normalized manner. Three-dimensional analysis of cerebellar brain slices was performed using the *z*-stack feature, and images were 3D rendered using the 3D rendering software vaa3d (Peng et al., 2014). Representative images shown in figures are digitally enhanced to increase the readability. All analyses were conducted by observers blinded to the experimental arm of the study.

2.12 | LC-ESI-MS/MS

EV pellets were diluted in 700 µL 1x PBS with 800 µL 1 N HCl:CH_3OH 1:8 (v/v), 900 µL $ChCl_3$ and 200 µg/mL of the antioxidant 2,6-di-tert-butyl-4-methylphenol (BHT; Sigma-Aldrich). 3 µL of SPLASH LIPIDOMIX Mass Spec Standard (cat. #330707, Avanti Polar Lipids), 3 µL of Ceramides, and 3 µL of Hexosylceramides Internal Standards (cat. #5040167 and cat. #5040398, AB SCIEX) were added to the extract mix. The organic fraction was evaporated at room temperature using the Savant Speed-vac spd111v (Thermo Fisher), and the remaining lipid pellet was reconstituted in 100% ethanol. Lipid species were analysed by liquid chromatography-electrospray ionization tandem mass spectrometry (LC-ESI-MS/MS) on a Nexera X2 UHPLC system (Shimadzu) coupled with hybrid triple quadrupole/linear ion trap mass spectrometer (6500+ QTRAP system; AB SCIEX). Chromatographic separation was performed on a XBridge amide column (150 mm × 4.6 mm, 3 × 5 µm; Waters) maintained at 35°C using mobile phase A [1 mM ammonium acetate in water-acetonitrile 5:95 (v/v)] and mobile phase B [1 mM ammonium acetate in water-acetonitrile 50:50 (v/v)] in the following gradient: (0–6 min: 0% B → 6% B; 6–10 min: 6% B → 25% B; 10–11 min: 25% B → 98% B; 11–13 min: 98% B → 100% B; 13–19 min: 100% B; 19–24 min: 0% B) at a flow rate of 0.7 mL/min which was increased to 1.5 mL/min from 13 min onward. Sphingomyelin (SM) and cholesteryl esters (CE) were measured in positive ion mode with a precursor scan of 184.1 and 369.4. Triglycerides (TG), diglycerides and monoglycerides were measured in positive ion mode with a neutral loss scan for one of the fatty acyl moieties. Phosphatidylcholine (PC), phosphatidylethanolamine (PE),

phosphatidylglycerol (PG), phosphatidylinositides (PI) and phosphatidylserines (PS) were measured in negative ion mode by fatty acyl fragment ions. Lipid quantification was performed by scheduled multiple reactions monitoring, the transitions being based on the neutral losses or the typical product ions as described above. The instrument parameters were as follows: Curtain Gas = 35 psi; Collision Gas = 8 a.u. (medium); IonSpray Voltage = 5500 V and -4500 V; Temperature = 550°C; Ion Source Gas 1 = 50 psi; Ion Source Gas 2 = 60 psi; Declustering Potential = 60 V and -80 V; Entrance Potential = 10 V and -10 V; Collision Cell Exit Potential = 15 V and -15 V. Peak integration was performed with the Multiquant™ software version 3.0.3. Lipid species signals were corrected for isotopic contributions (calculated with Python Molmass 2019.1.1) and were quantified based on internal standard signals and adhere to the guidelines of the Lipidomics Standards Initiative. Only the detectable lipid classes and fatty acyl moieties are reported in this manuscript.

2.13 | Cholesterol measurements

Cholesterol levels of BMDM-derived EVs were defined by using the Amplex Red Cholesterol Assay kit (Thermo Fisher) according to the manufacturer's instructions. Fluorescence was measured using the CLARIOstar PLUS microplate reader (BMG Labtech).

2.14 | Cholesterol depletion/repletion

IL-4-stimulated BMDM-derived EVs were depleted of cholesterol by incubation with 2.5% and 5% m/v MβCD for 1 h at 37°C. LPS-stimulated BMDM-derived EVs were enriched with cholesterol by incubating the EVs with 2.5% and 5% m/v MβCD/cholesterol complexes (molar mass 8:1) overnight at 37°C while shaking at 250 rpm. After cholesterol depletion/repletion, unincorporated MβCD and MβCD:cholesterol complexes were removed by means of SEC, and EVs were concentrated using Amicon 0.5 mL 10 kDa filters. Depletion/repletion of cholesterol was verified using the Amplex Red Cholesterol Assay kit.

2.15 | Quantitative PCR

EVs were lysed using QIAzol reagent (Qiagen) Next, small RNA was extracted using the *mir*Vana™ miRNA isolation kit (Ambion), according to the manufacturer's instructions. Subsequently cDNA was synthesized using the qScript cDNA synthesis kit (Quanta Biosciences) according to the manufacturer's instructions and stem loop primers listed in Table S1. Quantitative PCR was performed on a Quantstudio3 detection system (Applied Biosystems). Data were analysed using the comparative Ct method and normalized to U6. All miRNA primers used are listed in Table S1.

2.16 | EV uptake

EVs were fluorescently labelled with 1,1′-dioctadecyl-3,3,3′,3′-tetramethylindo-carbocyanine perchlorate (DiI; Sigma-Aldrich) for 30 min at 37°C. Next, unincorporated DiI was removed using SEC and samples were concentrated using the Amicon Ultra 0.5 mL 10 kDa filter. To investigate the effect of inhibiting specific EV uptake pathways, OPCs, either cultured on coverslips or not, were pre-incubated with Cytochalasin D, chlorpromazine hydrochloride, nystatin, imipramine hydrochloride, wortmannin, omeprazole and MβCD for 30 mins. Next, OPCs were exposed to 4×10^8 DiI-labelled EVs/mL for 3 h and subsequently washed with PBS to remove unincorporated DiI-labelled EVs. Thereafter, OPCs cultured on coverslips were fixed with 4% PFA for 20 min at room temperature, counterstained with DAPI (Sigma-Aldrich), imaged using the Leica DM2000 LED fluorescence microscope (Leica Microsystems), and analysed using ImageJ. Similarly, OPCs not cultured on coverslips were collected and analysed for fluorescence intensity using the FACS Calibur (BD Biosciences).

2.17 | Luciferase-based nuclear receptor reporter assay

To determine the ligation of liver X receptor (LXR) α and LXRβ, luciferase-based reporter assays were performed using the ONE-GloTM Luciferase Assay System kit (Promega). COS7 cells were transfected with bacterial plasmid constructs expressing luciferase under the control of the ligand-binding domain for LXRα or LXRβ, which were kindly provided by Prof. Dr. Bart Staels (Université de Lille, INSERM, France). Cells were grown to 60% confluency in 60 mm petri dishes and subsequently transfected with 1.8 μg plasmid DNA, including 0.2 μg pGAL4hLXRα or pGAL4hLXRβ, 1 μg pG5-TK-GL3 and 0.6 μg pCMV-β-galactosidase. JetPEI (Polysciences) was used as transfection reagent. After overnight incubation, transfected cells were seeded at a density of 10,000 cells/well in a 96-well plate in DMEM medium enriched with 50 U/mL penicillin and 50 U/mL streptomycin, and treated

with vehicle, BMDM-derived EVs, or T0901317 for 24 h. Following treatment, cells were lysed in lysis buffer (25 mM Glycyl-Glycine, 15 mM $MgSO_4$, 4 mM EGTA, and 1x Triton, all from Sigma-Aldrich). To correct for transfection efficacy, β-galactosidase activity was measured using cell lysate (10%) in β-gal buffer, consisting of 20% 2-Nitrophenyl β-D-galactopyranoside (ONGP; Sigma-Aldrich) and 80% Buffer-Z (0.1 M Na_2HPO_4, 10 mM KCl, 1 mM $MgSO_4$, and 3.4 µL/mL 2-mercaptoethanol; all from Sigma-Aldrich). Luminescence and absorbance (410 nm) were measured using the CLARIOstar PLUS microplate reader.

2.18 | Statistical analysis

Data were statistically analysed using GraphPad Prism v8 and are reported as mean ± SEM. The D'Agostino and Pearson omnibus normality test was used to test for normal distribution. When datasets were normally distributed, an ANOVA (Tukey's post hoc analysis) or two-tailed unpaired Student's *t*-test (with Welch's correction if necessary) was used to determine statistical significance between groups. If datasets did not pass normality, the Kruskal-Wallis or Mann-Whitney analysis was applied. p values < 0.05 were considered to indicate a significant difference (*, $p < 0.05$; **, $p < 0.01$; ***, $p < 0.001$).

3 | RESULTS

3.1 | Extracellular vesicles released by RAMs improve OPC differentiation

Macrophages display tremendous phenotypical plasticity in neurological disorders, a reflection of dynamic intracellular and environmental changes (Bogie et al., 2020). To date, however, the molecular mechanisms and factors that drive the harmful and benign effector functions of macrophages in CNS disorders remain poorly understood. By exposing OPC cultures to conditioned medium of naive macrophages (M0), DAMs, or RAMs, we here assessed whether the secretome of DAM and RAMs impacts OPC maturation. Fluorescent staining demonstrated an increased ratio of the mature OLN marker MBP over the pre-OLN marker O4 in OPC cultures exposed to conditioned medium of RAMs (Figure 1a-c), suggesting increased OLN differentiation. To confirm enhanced maturation of OPCs at a morphological level, Sholl analysis was performed. Here, OPCs exposed to the secretome of RAMs displayed an increased number of dendrite branches as well as a more complex dendrite branch geometry (Figure 1d,e), morphological characteristics typically associated with enhanced OLN maturation (Livesey et al., 2016). Surprisingly, conditioned medium of DAMs did not impact the MBP/O4 ratio and morphological parameters in OPCs (Figure 1b–f). Altogether, these findings show that RAM-secreted soluble factors, at least partially, enhance OPC differentiation in vitro.

Emerging evidence points towards the pathophysiological significance of macrophage-derived EVs in the initiation and resolution of chronic inflammatory disorders (Jiang et al., 2022; Liu et al., 2021; Long et al., 2021). To define whether EVs underlie the reparative impact of RAMs on OPC maturation (Figure 1), OPCs were exposed to EVs isolated from naive macrophages, DAMs or RAMs (experimental design in Figure S1a). First, EVs were characterized according to the "Minimal Information for Studies of Extracellular Vesicles (MISEV)" guidelines (Witwer et al., 2021). Transmission electron microscopy demonstrated EVs displaying the typical spherical and cup-shape morphology and size (Figure S1b,c). Nanoparticle Tracking Analysis (NTA) further established similar distribution curves of EVs released by naive macrophages, DAMs and RAMs, with the majority of EVs displaying a particle size ranging from 50 to 150 nm (Figure S1d). Finally, immunoblotting showed that all EV isolates were positive for CD81 and Flottilin1, while lacking the endoplasmic marker GRP94 (Figure S1e). Collectively, these findings confirm the isolation of small EVs. Having established the efficient isolation of EVs from macrophages, we next assessed their impact on OPC differentiation. Mirroring the pro-regenerative impact of the RAM secretome, fluorescent staining demonstrated that EVs released by RAMs enhanced OPC maturation, evidenced by an increased MBP/O4 ratio (Figure 1g,h). Consistent with enhanced OPC maturation, Sholl analysis demonstrated higher dendrite branch numbers, ending radius and complexity in OPCs exposed to EVs released by RAMs as compared to DAM-derived EVs (Figure 1i-k). EVs released by naive macrophages and DAMs did not impact OPC maturation (Figure 1g,h), nor did dendrite ending radius differ in OPCs exposed to these EVs (Figure 1i-k). In aggregate, these findings indicate that RAMs promote the maturation of OPCs in vitro, at least partially, through the release of EVs.

3.2 | Extracellular vesicles released by RAMs improve remyelination

Given that EVs released by RAMs enhanced OPC differentiation, we next sought to define their impact on remyelination. Remyelination was first studied using ex vivo cerebellar brain slices that were demyelinated with lysolecithin and subsequently exposed to EVs isolated from naive macrophages, DAMs, and RAMs (experimental design in Figure 2a) (Bogie et al., 2020). Fluorescent staining demonstrated increased colocalization of myelin (MBP) and axons (neurofilament, NF) in brain slices treated with RAM-derived EVs, indicating enhanced axonal remyelination (Figure 2b,c). Improved remyelination was confirmed using

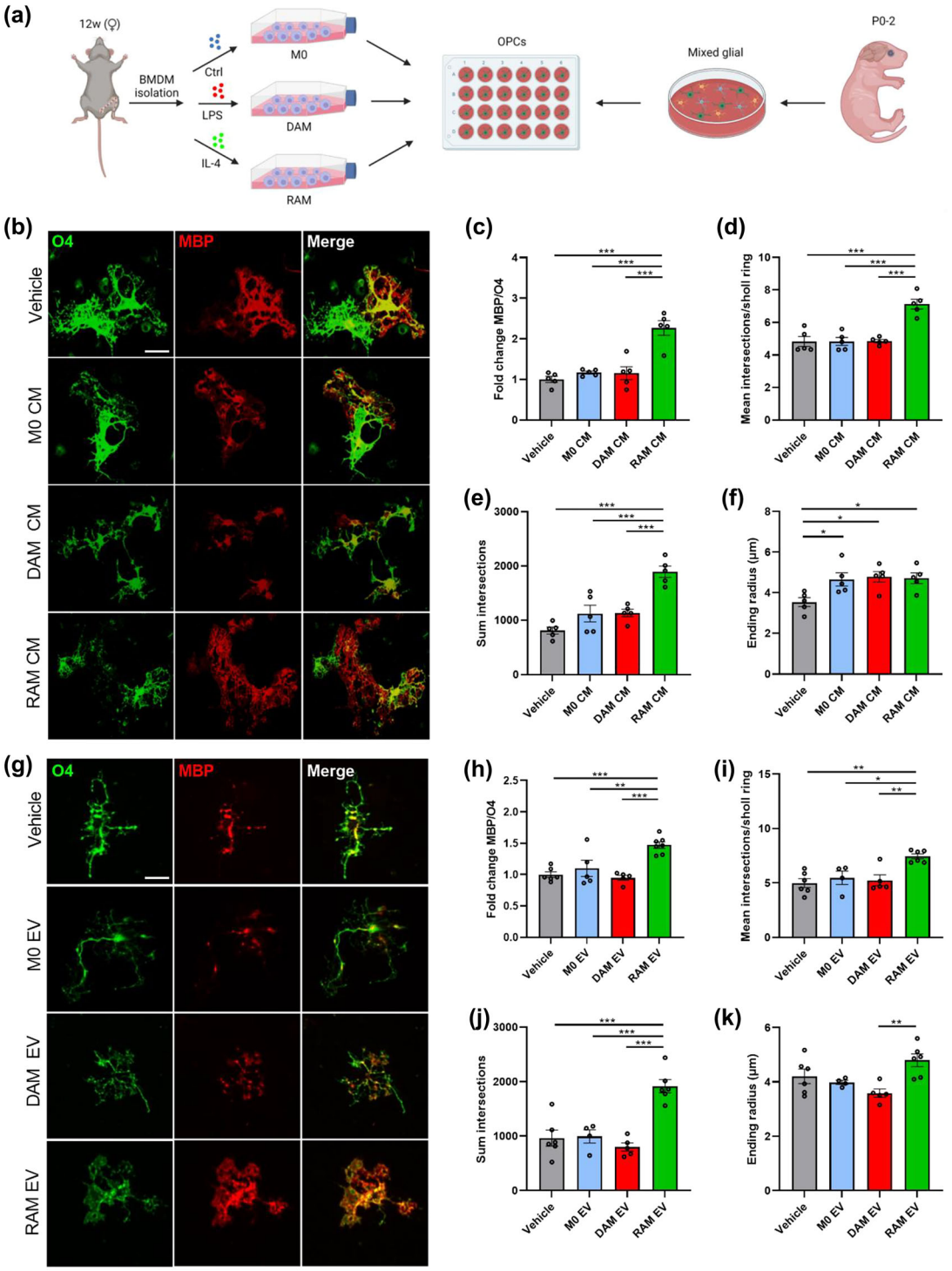

FIGURE 1 Extracellular vesicles released by RAMs improve OPC differentiation. (a) Schematic representation showing the isolation of oligodendrocyte precursor cells (OPCs) and their stimulation with conditioned medium (CM) and extracellular vesicles (EVs) released by naive macrophages (M0, PBS-treated), disease-associated macrophages (DAMs, LPS-stimulated), and repair-associated macrophages (RAMs, IL-4-stimulated). Created with biorender.com. (b–k) Representative immunofluorescent images (b, g) and quantification (c–f, h–k) of OPC maturation exposed to vehicle (BMDM culture medium (b–f), PBS (g–k)), conditioned medium (b–f) or EVs (g–k) isolated from M0, DAMs and RAMs for 6 days. OPCs were stained for MBP (mature oligodendrocyte) and O4 (premature oligodendrocyte), and differentiation was quantified by measuring the MBP/O4 ratio (c, h) or applying the Sholl analysis (mean interactions/ring, sum intersections, and ending radius; d–f, i–k). OPCs were treated with conditioned medium produced by 1.5×10^5 BMDMs or 4×10^8 EVs/mL. Scale bar, 25 µm. Results are pooled from or representative of four biological replicates ($n = 4$–6 cultures). Data are represented as mean ± SEM and statistically analysed using the one-way ANOVA test followed by Tukey's multiple comparison test. *, $p < 0.05$; **, $p < 0.01$; ***, $p < 0.001$.

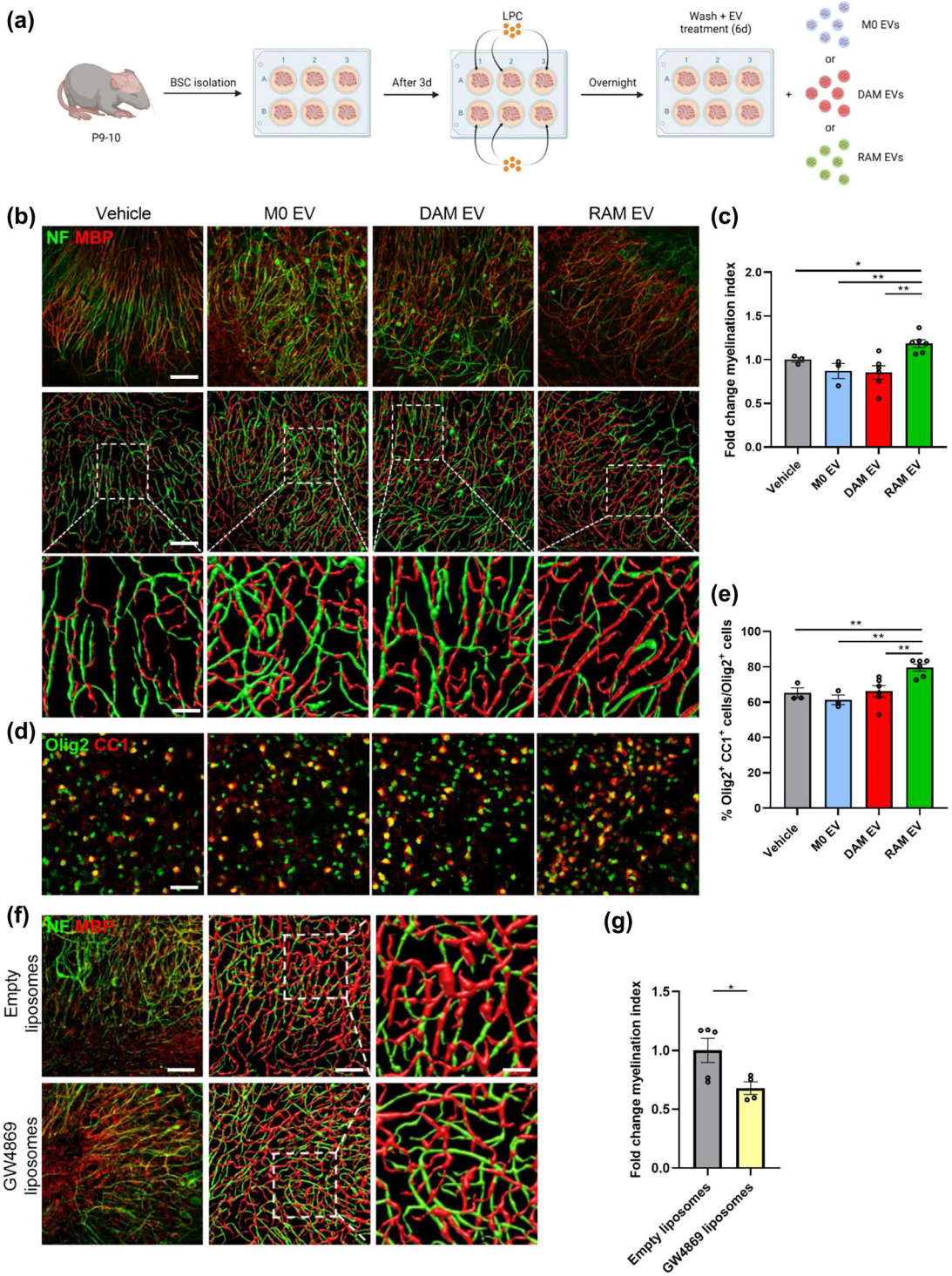

FIGURE 2 Extracellular vesicles released by RAMs improve remyelination in cerebellar brain slices. (a) Schematic representation showing the isolation and culture of cerebellar brain slices as well as their stimulation with vehicle (PBS), or extracellular vesicles (EVs) released by naive macrophages (M0, PBS-treated), disease-associated macrophages (DAMs, LPS-stimulated) and repair-associated macrophages (RAMs, IL-4-stimulated). LPC = lysolecithin, demyelinating compound. Created with biorender.com. (b, d) Representative images and three-dimensional reconstruction of immunofluorescent MBP/NF (b) and Olig2/CC1 (d) stains of cerebellar brain slices treated with vehicle or EVs isolated from M0, DAMs and RAMs. Slices were treated with 4×10^9 EVs/mL. Scale bars, 100 μm (b, (row 1, 2) d); 25 μm (b, row 3). (c) Relative number of MBP^+ NF^+ axons out of total NF^+ axons in cerebellar brain slices treated with vehicle or EVs released by M0, DAMs and RAMs ($n = 3$–6 slices). (e) Percentage $Olig2^+$ $CC1^+$ cells within the $Olig2^+$ cell population in cerebellar brain slices treated with vehicle or EVs released by M0, DAMs and RAMs ($n = 3$–6 slices). (f) Representative images and three-dimensional reconstruction of immunofluorescent MBP/NF of cerebellar brain slices treated with empty liposomes or GW4869 liposomes. Scale bars, 100 μm (column 1, 2); 25 μm (column 3). (g) Relative number of MBP^+ NF^+ axons out of total NF^+ axons in cerebellar brain slices treated with empty liposomes or GW4869 liposomes ($n = 4$–5 slices). Results are pooled from or representative of three independent experiments. Data are represented as mean ± SEM and statistically analysed using the Kruskal–Wallis test followed by Dunn's multiple comparison test (c, e) or the Mann-Whitney test (g). *, $p < 0.05$; **, $p < 0.01$.

three-dimensional reconstructions (Figure 2b). Akin to our in vitro findings, RAM-derived EVs increased the percentage of $CC1^+$ mature OLNs within $Olig2^+$ oligodendroglial lineage cells (Figure 2d,e). Remyelination efficiency and the percentage of $CC1^+$ $Olig2^+$ cells were not affected in brain slices exposed to EVs released by DAMs as well as naive macrophages (Figure 2b-e), similar to our in vitro OPC cultures. To further study the impact of EV biogenesis on endogenous remyelination, brain slices were exposed to GW4869, an inhibitor of EV biogenesis (Wang et al., 2014), or liposomes loaded with GW4869 to specifically target CNS-resident phagocytes (Ahsan et al., 2002). Here, we found that both pan- and phagocyte-specific inhibition of EV biogenesis hampered remyelination in brain slice cultures (Figure 2f,g; Figure S2a,c). Further, by replenishing brain slices that were depleted of resident phagocytes with DAMs and RAMs pre-treated with GW4869, we observed reduced endogenous remyelination (Figure S2b,d). Collectively, these findings point towards the importance of EVs released by phagocytes in endogenous remyelination, and provide evidence that EVs released by RAMs promote remyelination by enhancing the maturation of OPCs.

To evaluate the significance of these findings in vivo, the cuprizone-induced de- and remyelination model was used. Cuprizone feeding leads to reproducible toxic demyelination in distinct brain regions, the corpus callosum (CC) in particular. Upon cessation of cuprizone feeding, spontaneous remyelination occurs, as evidenced by increased MBP levels, a decreased g-ratio (the ratio of the inner axonal diameter to the total outer diameter), and higher percentage of $CC1^+$ $Olig2^+$ cells in the CC of mice 1 week after cessation of cuprizone feeding (5w+1) (Figure S3a-d). To study the impact of macrophage-derived EVs on remyelination, EVs were administrated intracerebroventricularly after demyelination. Consistent with their pro-regenerative impact in brain slices cultures, EVs released by RAMs enhanced MBP abundance in the CC of cuprizone animals as compared to animals exposed to vehicle or EVs released by naive macrophages and DAMs (Figure 3a-c). Accordingly, transmission electron microscopy showed a decreased g-ratio and increased percentage of myelinated axons in the CC of mice treated with EVs released by RAMs (Figure 3b,d,e). In particular, small diameter axons showed thicker myelin sheaths in mice that were treated with RAM-derived EVs (Figure S3e). Moreover, intracerebroventricular administration of RAM-derived EVs increased the number of mature OLNs, evidenced by an increased percentage of $CC1^+$ $Olig2^+$ cells. Again, EVs released by naive macrophages and DAMs did not affect axonal remyelination and the numbers of $CC1^+$ $Olig2^+$ cells (Figure 3b-e). To further elucidate the translational impact of our findings, a cuprizone experiment was performed in which EVs were administered intranasally. Similar to intracerebroventricular administration, daily intranasal administration of RAM-derived EVs resulted in an increased MBP abundance and a higher percentage of $CC1^+$ $Olig2^+$ cells in the CC of cuprizone animals as compared to mice exposed to vehicle or EVs derived from naive macrophages and DAMs (Figure S3f-h). Collectively, these findings indicate that EVs released by RAMs boost remyelination, likely through enhancing the intrinsic capacity of OPCs to mature into myelinating OLNs.

3.3 | Cholesterol abundance controls the impact of EVs released by macrophages on OPC maturation

Ample evidence indicates that OPC differentiation and remyelination cause a surge in lipid demand (Dimas et al., 2019; Hubler et al., 2018; Saher et al., 2005). Given that (1) EVs are carriers of lipids, (2) the importance of immunometabolism in driving macrophage effectors functions and (3) EV-associated lipids being acknowledged to affect neuropathological processes (Bogie et al., 2020; Goossens et al., 2019; Grey et al., 2015; Krämer-Albers et al., 2007; Oishi et al., 2017; Vanherle et al., 2020; Wang et al., 2012), we next assessed the impact of EV-associated lipids on remyelination. Here, we provide evidence that the lipid fraction of EVs released by RAMs markedly enhanced the MBP/O4 ratio as well as dendrite branch numbers and complexity of OPCs (Figure 4a–d; Figure 4a). Lipids within EVs released by naive macrophages and DAMs did not impact OPC maturation. To identify lipids involved in driving the regenerative impact of RAM-derived EVs, electrospray ionization tandem mass spectrometry (ESI-MS/MS) analysis was performed on EVs. Interestingly, while the vast majority of glycerolipids, glycerophospholipids and sphingolipids were unaltered in all EV subsets, EVs released by RAMs showed a marked increase in cholesteryl ester (CE) levels (Figure 4e). In-depth profiling did not identify changes in the relative abundance (% of class) of divergent fatty acid species within CE of RAM- and DAM-derived EVs, indicating an overall increase of all CE species (Figure 4f). Increased levels of CE, as well as free and total cholesterol, were confirmed using the Amplex Red Cholesterol Assay (Figure 4g). To validate alterations in EV-associated cholesterol in a physiologically relevant setting, we proceeded to evaluate the cholesterol content of EVs released by PBMCs from individuals with relapsing-remitting multiple sclerosis (RRMS). In line with the presence of active disease activity in these patients, our findings revealed a noticeable reduction in the cholesterol content of EVs derived from PBMCs of MS patients as compared to PBMCs of age- and gender-matched healthy controls (Figure 4h).

To establish whether increased cholesterol abundance underpins the regenerative impact of EVs released by RAMs, a cholesterol-depletion and -enrichment strategy using unloaded and cholesterol-loaded MβCD was applied (Experimental design in Figure 4i, j). MβCD efficiently depleted and enriched RAMs and DAMs of cholesterol, respectively (Figure S4b,h). As expected, EVs depleted of cholesterol showed a reduced particle size, while the size of those enriched in cholesterol was increased (Figures S1b,c and d S4c,i). Given that high levels of MβCD (5%) noticeably decreased the number of EVs, potentially due to cholesterol-associated changes in membrane integrity, we opted to continue with EVs modified with 2.5% MβCD and cholesterol-loaded MβCD (Figure S4d,j). Notably, cholesterol depletion and enrichment did not affect the uptake of EVs by

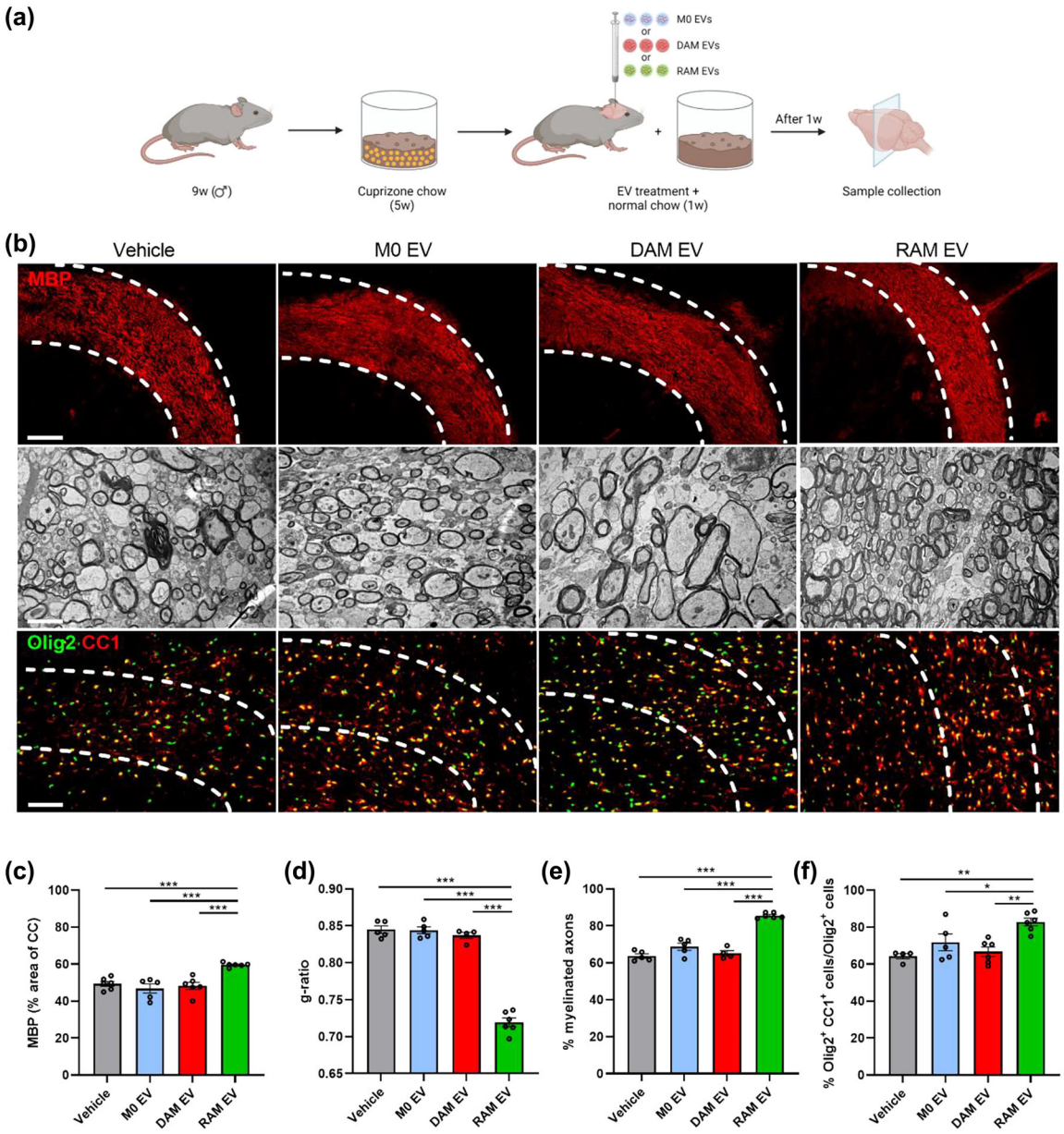

FIGURE 3 Extracellular vesicles released by RAMs enhance remyelination in the cuprizone model. (a) Schematic representation showing the experimental pipeline used to assess the impact of extracellular vesicles (EVs) released by naive macrophages (M0, PBS-treated), disease-associated macrophages (DAMs, LPS-stimulated), and repair-associated macrophages (RAMs, IL-4-stimulated) on remyelination in the cuprizone model. Created with biorender.com. (b) Representative images of immunofluorescent MBP and Olig2/CC1 stains and transmission electron microscopy analysis of the corpus callosum (CC) from mice treated intracerebroventricularly with vehicle (PBS) or EVs released by M0, DAMs and RAMs. The outer border of the CC is demarcated by the dotted line. Mice were injected with vehicle or EVs (1×10^9 EVs) after demyelination (5w), and analysis was performed during remyelination (5w+1). Scale bar, 200 μm (rows 1, 3) and 2 μm (row 2). (c) Quantification of the MBP^+ area of the CC from cuprizone mice treated with vehicle or EVs during remyelination (5w+1) ($n = 5$–6 animals, 3 images/animal). (d, e) Analysis of the g-ratio (the ratio of the inner axonal diameter to the total outer diameter, (d), and percentage myelinated axons (e) in CC from cuprizone mice treated with vehicle or EVs during remyelination (5w+1) ($n = 3$–5 animals, 3 images/animal, 100–150 axons/image). (f) Quantification of the percentage $Olig2^+$ $CC1^+$ cells out of total $Olig2^+$ cells in the CC of cuprizone animals treated with vehicle or EVs during remyelination (5w+1) ($n = 4$–6 animals, 3 images/animal). Data are represented as mean ± SEM and statistically analysed using the Kruskal–Wallis test followed by Dunn's multiple comparison test. *, $p < 0.05$; **, $p < 0.01$; ***, $p < 0.001$.

OPCs (Figure S4e,k), nor did it decrease protein levels or miRNAs levels known to be involved in OPC maturation (Figure S4f,g) (Buller et al., 2012; Dugas et al., 2010; Lau et al., 2008; Lecca et al., 2016; Tripathi et al., 2019; Wang et al., 2017; Zhao et al., 2010). In support of the importance of EV-associated cholesterol in driving OPC maturation, the pro-regenerative impact of EVs released by RAMs on OPC maturation and morphology was nullified upon cholesterol depletion (Figure 4k-n, Figure S4l). Vice versa, EVs released by DAMs gained the ability to promote OPC maturation once enriched with cholesterol, with values reaching those observed in OPC cultures exposed to non-modified EVs released by RAMs (Figure 4k-n, Figure S4l). To further elucidate the

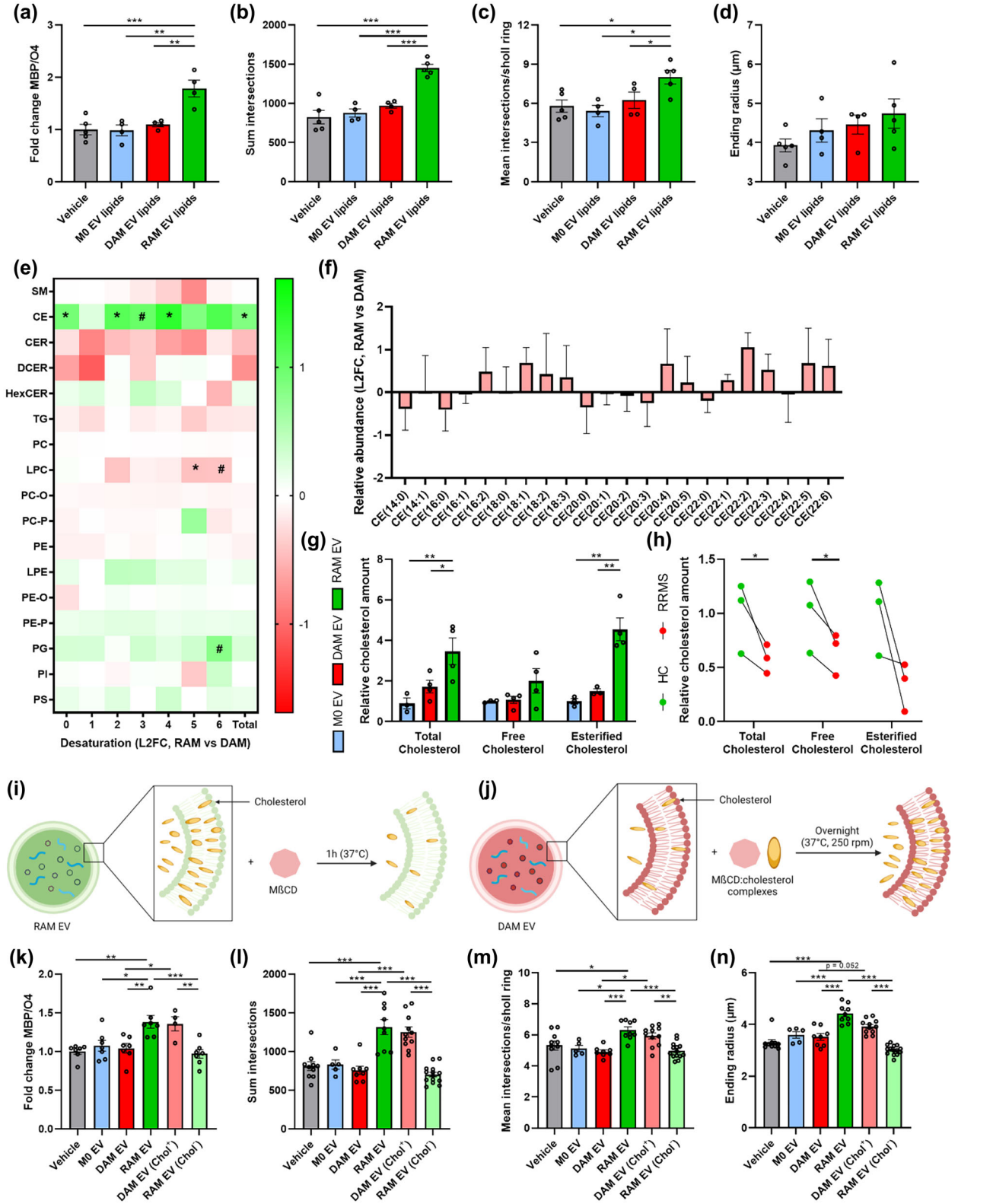

FIGURE 4 Cholesterol abundance controls the impact of EVs released by macrophages on OPC maturation. (a–d) Quantification of OPC maturation following 6-day exposure to lipids isolated from EVs released by naive macrophages (M0, PBS-treated), disease-associated macrophages (DAMs, LPS-stimulated) and repair-associated macrophages (RAMs, IL-4-stimulated). OPCs were stained for MBP (mature oligodendrocyte) and O4 (premature oligodendrocyte), and differentiation was quantified by measuring the MBP/O4 ratio (a) or applying the Sholl analysis (mean interactions/ring, sum intersection, and ending radius; b–d). OPCs were treated with 4×10^8 EVs/mL ($n = 4$–5 cultures). (e) Liquid chromatography electrospray tandem mass spectrometry (LC-ESI-MS/MS) analysis to measure lipid species of EVs released by DAMs and RAMs ($n = 3$ isolates). Data are depicted as $\log_2$ fold change (L2FC). SM, sphingomyelin; CE, cholesterol esters; TG, triglycerides; (D/H)CER, (dihydro/hexosyl)ceramide; (L)PC(-O/-P), (lyso,-alkyl/-alkenyl) phosphatidylcholine; (L)PE(-O/-P), (lyso, -alkyl/-alkenyl) phosphatidylethanolamine; PG, phosphatidylglycerol and PI, phosphatidylinositol. (f) Relative

(Continues)

FIGURE 4 (Continued)

abundance of fatty acyl moieties within CE group is shown (RAM EVs vs. DAM EVs). Data are depicted as L2FC ($n = 3$ isolates). (g, h) Quantification of total cholesterol, free cholesterol, and esterified cholesterol in EVs isolated from M0, DAMs, and RAMs (g, $n = 3$–4 isolates) and EVs isolated from peripheral blood mononuclear cells (PBMCs) of healthy controls (HC, $n = 3$ individuals) and relapsing-remitting multiple sclerosis patients (RRMS) (h, $n = 3$ patients). With respect to the latter, age-matched and gender-matched comparisons are depicted. i, j) Schematic representation of the experimental pipeline used for cholesterol depletion (h) and enrichment (i) of EVs released by RAMs and DAMs, respectively. Created with biorender.com. (k–n) Quantification of OPC maturation following 6 days exposure to EVs isolated from M0, DAMs and RAMs, as well as EVs isolated from DAMs and RAMs that were enriched ($Chol^+$) with or depleted ($Chol^-$) of cholesterol, respectively. OPCs were stained for MBP (mature oligodendrocyte) and O4 (premature oligodendrocyte), and differentiation was quantified by measuring the MBP/O4 ratio (j) or applying the Sholl analysis (mean interactions/ring, sum intersection and ending radius; k–m). OPCs were treated with 4×10^8 EVs/mL ($n = 5$–12 cultures). All results are pooled from three biological replicates. Data are represented as mean ± SEM and statistically analysed using the one-way ANOVA test followed by Tukey's multiple comparison test (a–d, j–m), the Mann-Whitney test (f), and the Kruskal–Wallis test followed by Dunn's multiple comparison test (g). #, $p < 0.1$, *, $p < 0.05$; **, $p < 0.01$; ***, $p < 0.001$.

importance of cholesterol in driving OPC maturation, OPC cultures were exposed to cholesterol. Cholesterol supplementation enhanced OPC maturation, as demonstrated by an increased MBP/O4 ratio and increased complexity of OPCs exposed to cholesterol (Figure S4m-q). Altogether, these findings highlight that EVs are essential for cholesterol trafficking and that changes in cholesterol abundance dictate, at least partially, the pro-regenerative impact of EVs released by macrophages on OPC maturation.

3.4 | Cholesterol abundance dictates the impact of EVs released by macrophages on remyelination

To provide evidence that the cholesterol content in macrophage-derived EVs impacts remyelination in a physiological setting, cerebellar brain slices and cuprizone mice were exposed to EVs released by DAMs and RAMs, which were either depleted or enriched in cholesterol. Consistent with our in vitro findings, we found that EVs released by RAMs lose their reparative features in brain slices once depleted of cholesterol as compared to their non-modified equivalents, evidenced by reduced colocalization of MBP with NF and lower numbers of $CC1^+$ $Olig2^+$ mature OLNs (Figure 5a-d). Mirroring these findings, EVs released by DAMs increased axonal remyelination and OLN numbers following cholesterol enrichment as compared to their non-modified counterparts (Figure 5a-d). Similar to brain slice cultures, intracerebroventricular administration of modified and non-modified EVs confirmed the vital role of cholesterol in driving the reparative features of EVs. Specifically, cholesterol depletion of EVs released by RAMs nullified their beneficial impact on remyelination in the CC as evidenced by increased MBP levels, a higher percentage of myelinated axons, and a decreased g-ratio. Vice versa, cholesterol enrichment of DAM-derived EVs increased their beneficial impact on these pathological parameters (Figure 5e-h, Figure S5a,b). Accordingly, a lower and higher percentage of $CC1^+$ $Olig2^+$ mature OLNs was observed in the CC of cuprizone mice treated with cholesterol-depleted RAM EVs and cholesterol-enriched DAM EVs, respectively, as compared to non-modified equivalents (Figure 5e-h, Figure S5a,b). In both models, neuropathological changes observed after exposure to MβCD-modified EVs matched those seen after treatment with non-modified EVs released by phenotypically divergent macrophage subsets, further emphasizing the importance of cholesterol in dictating the repair-promoting features of macrophage-derived EVs. To elucidate whether the abundance of cholesterol in EVs controls the regenerative properties of other brain cell populations as well, cerebellar brain slice cultures were exposed to astrocyte-derived EVs, which were either depleted or enriched with cholesterol, or left unmodified. Interestingly, we found that cholesterol enrichment and depletion of astrocyte-derived EVs promoted and suppressed remyelination, respectively (Figure S5c–f). Collectively, these findings argue that EVs are cholesterol traffickers during remyelination and that cholesterol abundance underlies the reparative properties of EVs in demyelinated lesions, irrespective of the cellular source of these EVs.

3.5 | Pharmacological inhibition of direct membrane fusion using omeprazole counters the pro-regenerative impact of EVs released by RAMs

EV uptake and incorporation by recipient cells can ensue in several functionally divergent manners that are likely to impact cellular physiology differently (Figure 6a and (Kalluri & LeBleu, 2020)). To study the molecular mechanisms that drive the uptake of macrophage-derived EVs by OPCs, we applied pharmacological inhibitors targeting different EV uptake pathways. We show that cytochalasin D (receptor-mediated endocytosis), chlorpromazine (clathrin-mediated endocytosis), MβCD (lipid raft-mediated endocytosis), and omeprazole (direct membrane fusion) attenuate the uptake of RAM-derived EVs by OPCs, with omeprazole having the most prominent impact (Figure 6b). However, despite multiple molecular processes being involved in the uptake of EVs by OPCs, solely omeprazole counteracted the beneficial impact of RAM-derived EVs on OPC maturation (Figure 6c-f, Figure S6a). These findings suggest that direct membrane fusion of EVs with the cell membrane of OPCs drives the regenerative impact of RAM-derived EVs. Nonetheless, given potential off-target effects of omeprazole, as well as the other pharmacological inhibitors used, additional experiments are required to fully elucidate the molecular mechanisms involved. Alongside direct membrane fusion, we and others demonstrated that the formation of cholesterol metabolites promotes OPC maturation and

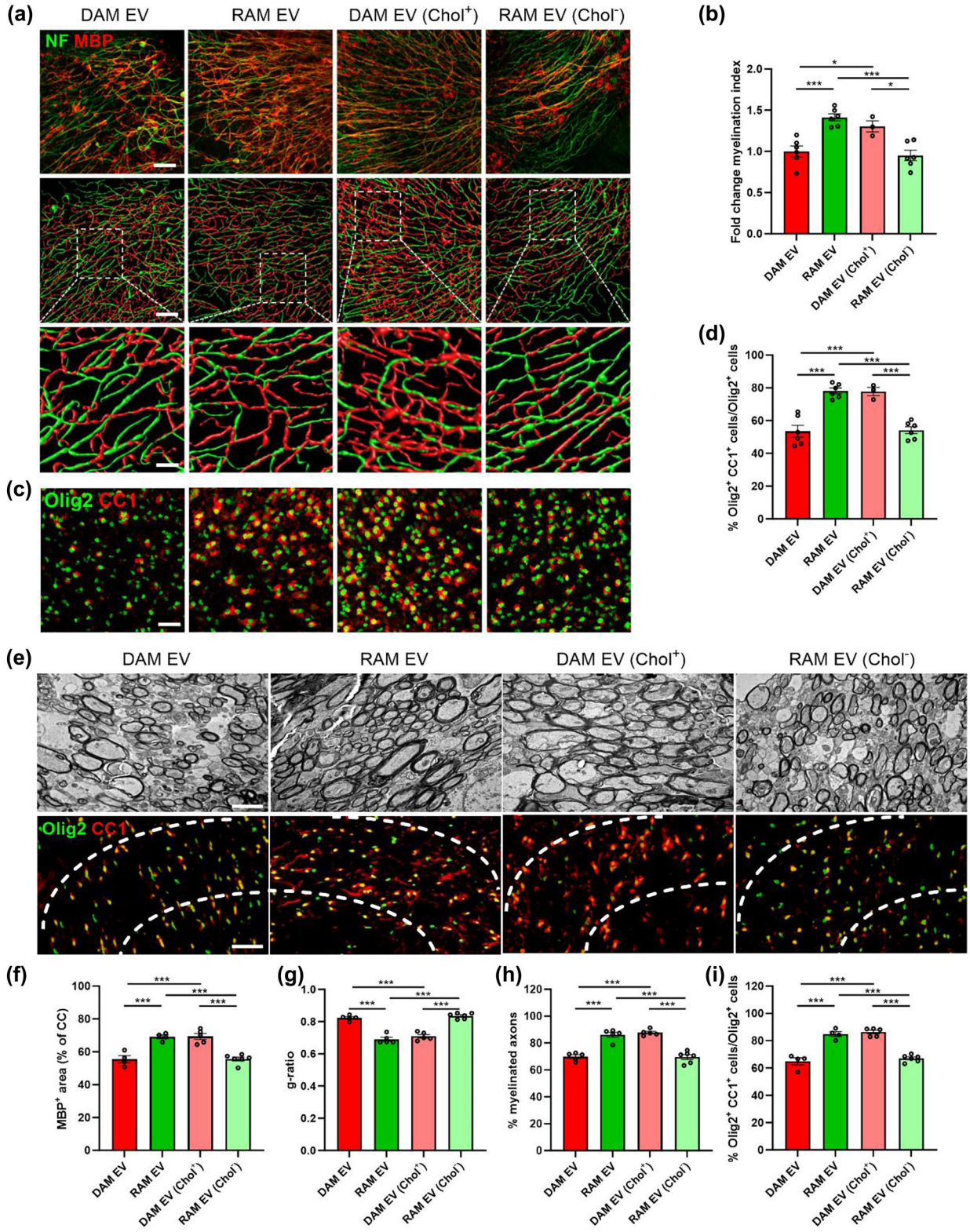

FIGURE 5 Cholesterol abundance controls the impact of EVs released by macrophages on remyelination. (a–d) Representative images, three-dimensional reconstruction, and quantification of immunofluorescent MBP/NF (a, b) and Olig2/CC1 stains (c, d) of cerebellar brain slices treated with vehicle or EVs released by disease-associated macrophages (DAMs, LPS-stimulated), and repair-associated macrophages (RAMs, IL-4-stimulated), as well as EVs released by DAMs and RAMs that were enriched ($Chol^+$) with or depleted ($Chol^-$) of cholesterol, respectively. Relative number of MBP^+ NF^+ axons out of total NF^+ axons (b) and percentage $Olig2^+$ $CC1^+$ cells within the $Olig2^+$ cell population (d) in cerebellar brain slices treated with vehicle or EVs is shown ($n = 3$–6 slices). Slices were treated with 4×10^9 EVs/mL. Scale bars, 100 μm (a (row 1 and 2), c); 25 μm (a (row 3)). (e) Representative images of transmission electron microscopy analysis and immunofluorescent Olig2/CC1 stains of the corpus callosum (CC) from mice treated with vehicle or EV subsets. The outer border of the CC is demarcated by the dotted line. Mice were intracerebroventricularly injected with vehicle or EVs (1×10^9 EVs/mL) after demyelination (5w),

(Continues)

FIGURE 5 (Continued)

and analysis was done during remyelination (5w+1). Scale bar, 200 μm (rows 1, 3) and 2 μm (row 2). (f) Quantification of the MBP^+ area of the CC from cuprizone mice treated with vehicle or EVs during remyelination (5w+1) ($n = 4–6$ animals, 3 images/animal). (g, h) Analysis of the g-ratio (the ratio of the inner axonal diameter to the total outer diameter, (g), and percentage of myelinated axons (h) in CC from cuprizone mice treated with vehicle or EVs during remyelination (5w+1) ($n = 5–6$ animals, 3 images/animal, 100–150 axons/image). (i) Quantification of the percentage $Olig2^+$ $CC1^+$ cells out of total $Olig2^+$ cells in the CC of cuprizone animals treated with vehicle or EVs during remyelination (5w+1) ($n = 4–6$ animals, 3 images/animal). Data are represented as mean ± SEM and statistically analysed using the Kruskal–Wallis test followed by Dunn's multiple comparison test. *, $p < 0.05$; **, $p < 0.01$; ***, $p < 0.001$.

remyelination by activating the cholesterol-sensing LXRs (Nelissen et al., 2012; Xu et al., 2014). However, by using nuclear receptor luciferase reporter assays, we found that control and modified EVs released by RAMs and DAMs did not enhance LXRα and LXRβ ligation (Figure 6Sb,c). In aggregate, these results suggest that RAM-derived EVs promote OPC maturation by directly incorporating cholesterol in the membrane of OPCs.

4 | DISCUSSION

Macrophages display tremendous functional diversity in CNS disorders, being involved in seemingly opposing processes such as neurodegeneration and remyelination (Aydınlı et al., 2022; Bogie et al., 2020; Marschallinger et al., 2020; Miron et al., 2013). Here, we report that RAMs promote OPC maturation and improve remyelination through the release of EVs. Lipidomic analysis revealed that EVs released by RAMs contained higher cholesterol levels, a steroid whose importance in remyelination has been well-established (Mathews et al., 2014; Saher et al., 2005). Cholesterol depletion counteracted the benign impact of EVs released by RAMs on OPC maturation and remyelination. Accordingly, cholesterol enrichment rendered DAM-derived EVs reparative, stipulating the crucial role of EV-associated cholesterol in remyelination, which we found to be directly incorporated into the membrane of OPCs via membrane fusion. Collectively, our findings show that EVs act as cholesterol traffickers in the CNS and that cholesterol abundance underlies, at least partially, their pro-remyelinating properties in demyelinated lesions.

We provide evidence that RAMs promote OPC differentiation in vitro and enhance remyelination ex vivo and in vivo through the release of soluble factors and EVs. Consistent with our findings, other studies defined that phagocytes can release soluble factors that promote CNS remyelination (Boyles et al., 1989; Butovsky et al., 2006; Miron et al., 2013; Yuen et al., 2013). Specifically, a phenotypic switch of disease- to repair-associated microglia was found to coincide with elevated levels of pro-regenerative activin-A, resulting in enhanced remyelination (Miron et al., 2013). Furthermore, repair-associated microglia, which were induced by IL-4, boost oligodendrogenesis in an autoimmune-induced demyelination model via the production of IGF-I (Butovsky et al., 2006). Ample evidence further indicates that EVs can have regenerative properties in the CNS and periphery (Guo et al., 2020; Herman et al., 2022; Hervera et al., 2018; Lombardi et al., 2019). Of particular interest, Lombardi et al. demonstrated that microglia co-cultured with immunosuppressive mesenchymal stem cells or stimulated with IL-4 release EVs that promote remyelination, either directly by affecting OPC physiology or indirectly by promoting the formation of reparative astrocytes (Lombardi et al., 2019). Our results now extend these findings by showing that disease-resolving peripheral macrophages, despite differing in their ontogeny and function compared to microglia (Ajami et al., 2011; Chrast et al., 2011; Goldmann et al., 2016; Mildner et al., 2007), promote remyelination through the release of EVs as well. Remarkably, while it was previously described that microglia activated by IFNγ hamper OPC maturation and remyelination (Butovsky et al., 2006), we showed that EVs released by DAMs did not negatively impact these processes. Based on the latter findings, one could speculate that DAMs negatively impact CNS repair through direct physical interactions with OPCs, while the detrimental effects of inflammatory microglia may stem from their secretome. Nevertheless, it is important to emphasize that the polarization of BMDMs into RAM and DAM phenotypes, as employed in our study, serves as an in vitro model aimed at mimicking the disease-promoting and -resolving macrophage profiles observed in CNS disorders (Bogie et al., 2020; Butovsky et al., 2006; Lombardi et al., 2019; Miron et al., 2013). Hence, this experimental model may not fully capture the diversity of macrophage subsets and phenotypes present in a physiological context. Therefore, further investigations are warranted to establish the biological relevance of EVs derived from DAMs and RAMs in a naturally occurring physiological context.

We show that cholesterol abundance in EVs released by macrophages is an essential determinant of their pro-remyelinating impact in the CNS, with higher cholesterol levels more efficiently promoting remyelination. Accordingly, cholesterol is well-known to be the rate-limiting step in myelin biogenesis, and up to 80% of CNS cholesterol can be found in myelin (Björkhem et al., 2010; Dietschy, 2009; Saher et al., 2005). In the context of remyelination, ample evidence indicates that changes in the level and synthesis of cholesterol and its metabolites markedly impact remyelination efficacy. First, an elevated expression of genes involved in cholesterol metabolism was previously observed in oligodendroglial lineage cells during remyelination (Voskuhl et al., 2019). Second, dietary cholesterol and 8,9-unsaturated sterols enhance the differentiation of OPCs, thereby promoting remyelination (Berghoff et al., 2017; Hubler et al., 2018). Consistent with these findings, our current study confirms the protective impact of cholesterol supplementation on OPC maturation. However, it remains unclear whether cholesterol supplementation directly affects OPC maturation or if its incorporation into complex macro-/carrier-molecules (e.g., lipoproteins or EVs), either through

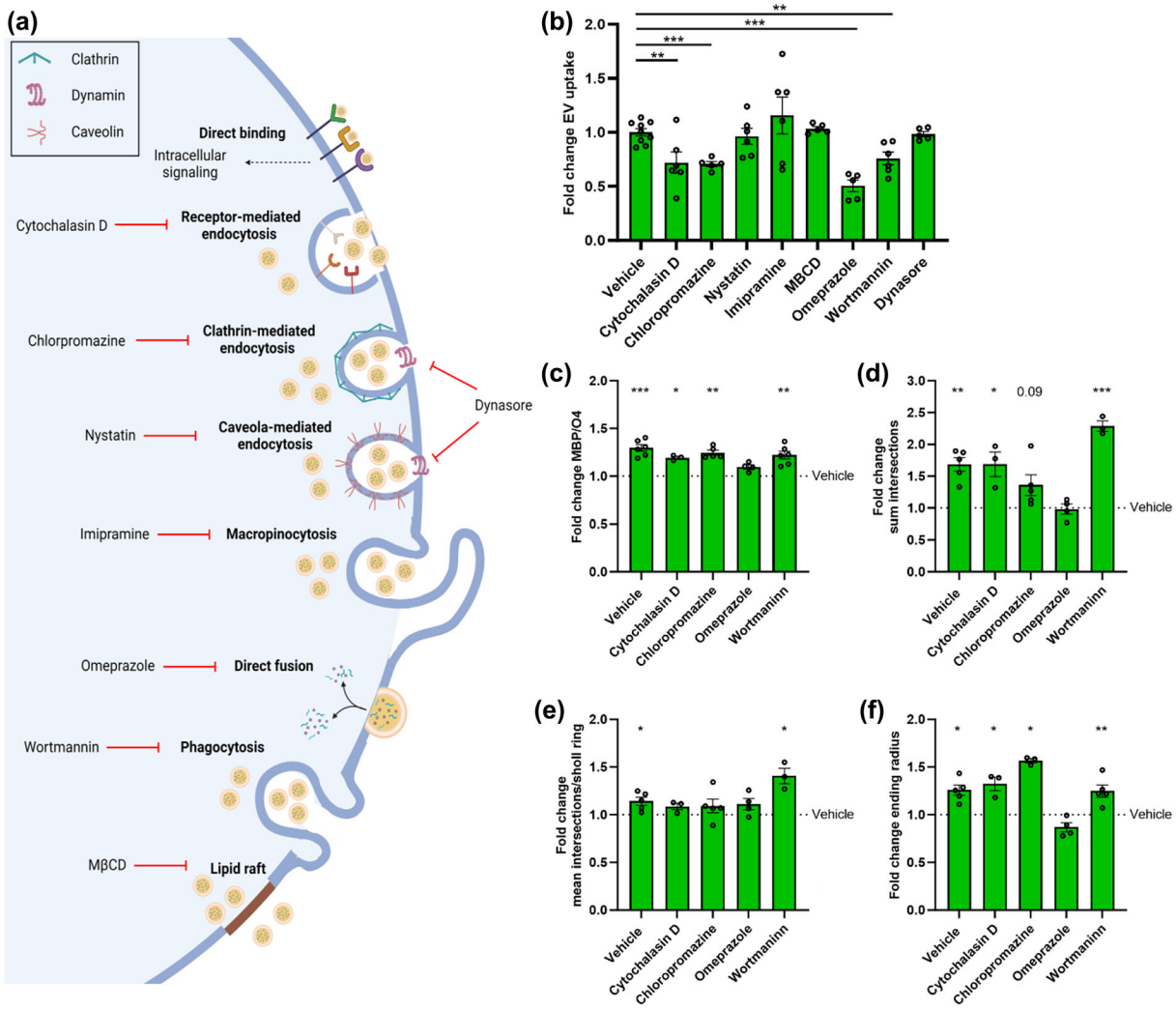

FIGURE 6 Pharmacological inhibition of direct membrane fusion using Omeprazole counters the regenerative impact of EVs released by RAMs. (a) Schematic representation showing routes of extracellular vesicles (EV) uptake and their associated inhibitors. Created with biorender.com. (b) Internalization of DiI-labelled EVs released by repair-promoting macrophages (RAMs, IL-4-stimulated) by OPCs pre-treated for 30 min with inhibitors of receptor-mediated endocytosis (cytochalasin D, 10 μM), clathrin-mediated endocytosis (chloropromazine, 50 μM), caveola-mediated endocytosis (nystatin, 25 μM), macropinocytosis (imipramine, 5 μM), direct fusion (omeprazole, 50 μM), phagocytosis (wortmannin, 500 nM), lipid raft-mediated uptake (methyl-β-cyclodextrin, 1% v/v) and dynamin-mediated endocytosis (dynasore, 20 μM). OPCs were exposed for 3 h to 4×10^8 EVs/mL ($n = 5$–9 cultures). (c–f) Quantification of OPC maturation following 6 days exposure to EVs isolated from RAMs and cytochalasin D, chloropromazine, omeprazole or wortmaninn. OPCs were stained for MBP (mature oligodendrocyte) and O4 (premature oligodendrocyte), and differentiation was quantified by measuring the MBP/O4 ratio (c; $n = 4$ cultures) or applying the Sholl analysis (mean interactions/ring, sum intersection and ending radius; D–F; $n = 5$ cultures). Quantification was represented as fold change of OPCs treated with RAM-derived EVs, compared to vehicle-treated OPCs. Dotted line represents vehicle-treated OPCs. OPCs were treated with 4×10^8 EVs/mL. All results are pooled from three biological replicates. Data are represented as mean ± SEM and statistically analysed using the Kruskal–Wallis test followed by Dunn's multiple comparison test (b), and the one-way ANOVA test followed by Tukey's multiple comparison test (c–f). *, $p < 0.05$; **, $p < 0.01$; ***, $p < 0.001$.

cellular or non-cellular mechanisms, is a necessary prerequisite for its pro-regenerative effects. Third, elevated cholesterol uptake promotes mTOR kinase activity in OPCs, thereby enhancing cholesterol synthesis and their maturation (Mathews & Appel, 2016). Finally, decreased cholesterol levels in the CNS of MS patients are associated with severe demyelination, which might well relate to perturbed remyelination in these patients (Evangelopoulos et al., 2022). How cholesterol mediates OPC maturation and remyelination remains poorly understood. However, there is now evidence that its mode of action relies on the lesion stage. While acute demyelinated lesions seem to rely on cholesterol recycling to enhance remyelination, chronic demyelinated lesions depend on increased local cholesterol synthesis in order to drive CNS repair (Berghoff et al., 2021a, 2021b). Given the abundance of macrophages in acute demyelinated lesions, this concept provides a molecular rationale for EVs acting as cholesterol traffickers and promoting endogenous OPC maturation and remyelination in active lesions, which often show signs of repair (Brück et al., 1997, 2003; Erickson, 2008; Staugaitis et al., 2012). It also argues for cholesterol-rich EVs, such as those released by RAMs, being of

therapeutic interest to boost remyelination, especially in chronic lesions which are generally devoid of macrophages and microglia (Hagemeier et al., 2012; Hanafy & Sloane, 2011; Wolswijk, 2002).

Horizontal lipid flux is essential in supplying OPCs with cholesterol for developmental myelination and remyelination (Berghoff et al., 2022). With respect to the latter, horizontal transfer of recycled cholesterol from astrocytes to OLNs via lipoproteins is a major feature of normal brain development and myelination (Camargo et al., 2017; Werkman et al., 2021). Our findings now indicate that macrophage-derived EVs are vital traffickers of cholesterol in demyelinating disorders as well, thereby closely monitoring CNS repair. Accordingly, other studies defined the importance of EVs in trafficking of lipids in neurodegenerative disorders, with EV-associated monosialogangliosides, phospholipids and ceramide analogues affecting amyloid-beta oligomerization, α-synuclein pathology, and neuroinflammation (Grey et al., 2015; Hoshino et al., 2013; Ikeda et al., 2011; Takasugi et al., 2015; Thomas & Salter, 2010). Guided by lipidomic analysis, microglia-derived EVs from Alzheimer's disease patients were further shown to have increased levels of free cholesterol and decreased levels of docosahexaenoic acid-containing polyunsaturated fatty acids (Cohn et al., 2021). Finally, EV-associated sphingosine-1-phosphate derived from repair-associated microglia enhances OPC migration towards demyelinated lesions (Lombardi et al., 2019). Hence, while our findings identify EV-associated cholesterol as a key molecular determinant of the reparative features of RAMs, more research is warranted to assess whether other lipids, in concert with cholesterol, enhance OPC maturation and remyelination. On a related note, given that EVs carry other bioactive molecules, including cytokines, growth factors and miRNAs, which impact CNS homeostasis and repair (Li et al., 2021, 2022; Raffaele et al., 2021), a synergistic effect of cholesterol in combination with these factors cannot be excluded. Similarly, whereas our findings indicate that EVs released by RAMs directly impact OPC maturation in vitro, we cannot exclude that other cell, including astrocytes and neurons (Lombardi et al., 2019), indirectly control the regenerative impact of RAM-derived EVs on remyelination ex vivo and in vivo. Finally, although our findings strongly suggest that RAM-derived EVs enhance remyelination by directly incorporating cholesterol in the membrane of OPCs, further research using additional approaches and techniques is warranted to fully elucidate the involved mechanisms. Also, future studies should investigate the molecular changes that underpin the observed significance of membrane fusion. Notably, changes in cholesterol composition can impact membrane protein function and abundance (Grouleff et al., 2015), thereby potentially affecting membrane fusion of EVs.

In summary, our findings indicate that EVs released by RAMs enhance OPC maturation and remyelination through EV-associated cholesterol, which appears to be directly incorporated into the OPC membrane via direct membrane fusion. Our findings could help in designing novel therapeutic strategies, including the synthesis of cholesterol-enriched EVs or nanostructured lipid carriers, to support remyelination in demyelinating disorders.

AUTHOR CONTRIBUTIONS

Sam Vanherle: Conceptualization; Formal analysis; Investigation; Methodology; writing—original draft. **Jeroen Guns**: Conceptualization; formal analysis; investigation; Methodology; writing—review and editing. **Melanie Loix**: Formal analysis; investigation; methodology; writing—review and editing. **Fleur Mingneau**: Investigation; writing—review and editing. **Tess Dierckx**: Investigation; writing—review and editing. **Flore Wouters**: Investigation; Methodology; writing—review and editing. **Koen Kuipers**: Investigation; methodology; writing—review and editing. **Tim Vangansewinkel**: Investigation; methodology; writing—review and editing. **Esther Wolfs**: Investigation; methodology; resources; writing—review and editing. **Paula Pincela Lins**: Formal analysis; investigation; methodology; writing—review and editing. **Annelies Bronckaers**: Investigation; methodology; resources; writing—review and editing. **Ivo Lambrichts**: Investigation; methodology; resources; writing—review and editing. **Jonas Dehairs**: Formal analysis; investigation; methodology; software; writing—review and editing. **Johannes V. Swinnen**: Methodology; resources; writing—review and editing. **Sanne G.S. Verberk**: Investigation; methodology; writing—review and editing. **Mansour Haidar**: Investigation; methodology; writing—review and editing. **Jeroen F. J. Bogie**: Conceptualization; data curation; funding acquisition; resources; supervision; writing—original draft.

ACKNOWLEDGEMENTS

We thank L. Timmermans, M.P. Tulleners, K. Wauterickx and M. Jans for excellent technical assistance. The work was financially supported by the Research Foundation of Flanders (FWO Vlaanderen; 1S15519N, G099618FWO, 12J9119N, 1141920N and 11M1722N) and Interreg V-A EMR program (EURLIPIDS, EMR23). The funding agencies have no role in the design, analysis and writing of the article.

CONFLICT OF INTEREST STATEMENT

The authors declare no competing interests.

ORCID

Jeroen F. J. Bogie https://orcid.org/0000-0002-0016-1926

REFERENCES

Ahsan, F., Rivas, I. P., Khan, M. A., & Torres Suarez, A. I. (2002). Targeting to macrophages: Role of physicochemical properties of particulate carriers–liposomes and microspheres–on the phagocytosis by macrophages. *Journal of Controlled Release*, *79*, 29–40.

Ajami, B., Bennett, J. L., Krieger, C., McNagny, K. M., & Rossi, F. M. (2011). Infiltrating monocytes trigger EAE progression, but do not contribute to the resident microglia pool. *Nature Neuroscience*, *14*, 1142–1149.

Aydınlı, F., Er, S., & Kerman, B. E. (2022). Two phases of macrophages: Inducing maturation and death of oligodendrocytes in vitro co-culture. *Journal of Neuroscience Methods*, *382*, 109723.

Berghoff, S. A., Gerndt, N., Winchenbach, J., Stumpf, S. K., Hosang, L., Odoardi, F., Ruhwedel, T., Bohler, C., Barrette, B., Stassart, R., Liebetanz, D., Dibaj, P., Möbius, W., Edgar, J. M., & Saher, G. (2017). Dietary cholesterol promotes repair of demyelinated lesions in the adult brain. *Nature Communications*, *8*, 14241.

Berghoff, S. A., Spieth, L., & Saher, G. (2022). Local cholesterol metabolism orchestrates remyelination. *Trends in Neuroscience (Tins)*, *45*, 272–283.

Berghoff, S. A., Spieth, L., Sun, T., Hosang, L., Depp, C., Sasmita, A. O., Vasileva, M. H., Scholz, P., Zhao, Y., Krueger-Burg, D., Wichert, S., Brown, E. R., Michail, K., Nave, K. A., Bonn, S., Odoardi, F., Rossner, M., Ischebeck, T., Edgar, J. M., & Saher, G. (2021a). Neuronal cholesterol synthesis is essential for repair of chronically demyelinated lesions in mice. *Cell Reports*, *37*, 109889.

Berghoff, S. A., Spieth, L., Sun, T., Hosang, L., Schlaphoff, L., Depp, C., Duking, T., Winchenbach, J., Neuber, J., Ewers, D., Scholz, P., van der Meer, F., Cantuti-Castelvetri, L., Sasmita, A. O., Meschkat, M., Ruhwedel, T., Möbius, W., Sankowski, R., Prinz, M., … Saher, G. (2021b). Microglia facilitate repair of demyelinated lesions via post-squalene sterol synthesis. *Nature Neuroscience*, *24*, 47–60.

Björkhem, I., Leoni, V., & Meaney, S. (2010). Genetic connections between neurological disorders and cholesterol metabolism. *Journal of Lipid Research*, *51*, 2489–2503.

Bogie, J. F., Mailleux, J., Wouters, E., Jorissen, W., Grajchen, E., Vanmol, J., Wouters, K., Hellings, N., van Horssen, J., Vanmierlo, T., & Hendriks, J. J. (2017). Scavenger receptor collectin placenta 1 is a novel receptor involved in the uptake of myelin by phagocytes. *Scientific Reports*, *7*, 44794.

Bogie, J. F. J., Grajchen, E., Wouters, E., Corrales, A. G., Dierckx, T., Vanherle, S., Mailleux, J., Gervois, P., Wolfs, E., Dehairs, J., Van Broeckhoven, J., Bowman, A. P., Lambrichts, I., Gustafsson, J. Å., Remaley, A. T., Mulder, M., Swinnen, J. V., Haidar, M., Ellis, S. R., … Hendriks, J. J. A. (2020). Stearoyl-CoA desaturase-1 impairs the reparative properties of macrophages and microglia in the brain. *Journal of Experimental Medicine*, *217*, e20191660.

Boyles, J. K., Zoellner, C. D., Anderson, L. J., Kosik, L. M., Pitas, R. E., Weisgraber, K. H., Hui, D. Y., Mahley, R. W., Gebicke-Haerter, P. J., & Ignatius, M. J. (1989). A role for apolipoprotein E, apolipoprotein A-I, & low density lipoprotein receptors in cholesterol transport during regeneration and remyelination of the rat sciatic nerve. *Journal of Clinical Investigation*, *83*, 1015–1031.

Brück, W., Bitsch, A., Kolenda, H., Brück, Y., Stiefel, M., & Lassmann, H. (1997). Inflammatory central nervous system demyelination: Correlation of magnetic resonance imaging findings with lesion pathology. *Annals of Neurology*, *42*, 783–793.

Brück, W., Kuhlmann, T., & Stadelmann, C. (2003). Remyelination in multiple sclerosis. *Journal of the Neurological Sciences*, *206*, 181–185.

Buller, B., Chopp, M., Ueno, Y., Zhang, L., Zhang, R. L., Morris, D., Zhang, Y., & Zhang, Z. G. (2012). Regulation of serum response factor by miRNA-200 and miRNA-9 modulates oligodendrocyte progenitor cell differentiation. *Glia*, *60*, 1906–1914.

Butovsky, O., Landa, G., Kunis, G., Ziv, Y., Avidan, H., Greenberg, N., Schwartz, A., Smirnov, I., Pollack, A., Jung, S., & Schwartz, M. (2006). Induction and blockage of oligodendrogenesis by differently activated microglia in an animal model of multiple sclerosis. *Journal of Clinical Investigation*, *116*, 905–915.

Camargo, N., Goudriaan, A., van Deijk, A. F., Otte, W. M., Brouwers, J. F., Lodder, H., Gutmann, D. H., Nave, K. A., Dijkhuizen, R. M., Mansvelder, H. D., Chrast, R., Smit, A. B., & Verheijen, M. H. G. (2017). Oligodendroglial myelination requires astrocyte-derived lipids. *Plos Biology*, *15*, e1002605.

Cantuti-Castelvetri, L., Fitzner, D., Bosch-Queralt, M., Weil, M. T., Su, M., Sen, P., Ruhwedel, T., Mitkovski, M., Trendelenburg, G., Lütjohann, D., Möbius, W., & Simons, M. (2018). Defective cholesterol clearance limits remyelination in the aged central nervous system. *Science*, *359*, 684–688.

Chrast, R., Saher, G., Nave, K. A., & Verheijen, M. H. (2011). Lipid metabolism in myelinating glial cells: Lessons from human inherited disorders and mouse models. *Journal of Lipid Research*, *52*, 419–434.

Cohn, W., Melnik, M., Huang, C., Teter, B., Chandra, S., Zhu, C., McIntire, L. B., John, V., Gylys, K. H., & Bilousova, T. (2021). Multi-omics analysis of microglial extracellular vesicles from human Alzheimer's disease brain tissue reveals disease-associated signatures. *Frontiers in Pharmacology*, *12*, 766082.

Cooper, J. M., Wiklander, P. B., Nordin, J. Z., Al-Shawi, R., Wood, M. J., Vithlani, M., Schapira, A. H., Simons, J. P., El-Andaloussi, S., & Alvarez-Erviti, L. (2014). Systemic exosomal siRNA delivery reduced alpha-synuclein aggregates in brains of transgenic mice. *Movement Disorders*, *29*, 1476–1485.

Di Bello, I. C., Dawson, M. R., Levine, J. M., & Reynolds, R. (1999). Generation of oligodendroglial progenitors in acute inflammatory demyelinating lesions of the rat brain stem is associated with demyelination rather than inflammation. *Journal of Neurocytology*, *28*, 365–381.

Dierckx, T., Vanherle, S., Haidar, M., Grajchen, E., Mingneau, F., Gervois, P., Wolfs, E., Bylemans, D., Voet, A., Nguyen, T., Hamad, I., Kleinewietfeld, M., Bogie, J. F. J., & Hendriks, J. J. A. (2022). Phloretin enhances remyelination by stimulating oligodendrocyte precursor cell differentiation. *Proceedings of the National Academy of Sciences of the United States of America*, *119*, e2120393119.

Dietschy, J. M. (2009). Central nervous system: Cholesterol turnover, brain development and neurodegeneration. *Biological Chemistry*, *390*, 287–293.

Dimas, P., Montani, L., Pereira, J. A., Moreno, D., Trötzmüller, M., Gerber, J., Semenkovich, C. F., Köfeler, H. C., & Suter, U. (2019). CNS myelination and remyelination depend on fatty acid synthesis by oligodendrocytes. *Elife*, *8*, e44702.

Dugas, J. C., Cuellar, T. L., Scholze, A., Ason, B., Ibrahim, A., Emery, B., Zamanian, J. L., Foo, L. C., McManus, M. T., & Barres, B. A. (2010). Dicer1 and miR-219 are required for normal oligodendrocyte differentiation and myelination. *Neuron*, *65*, 597–611.

Erickson, B. J. (2008). Imaging of remyelination and neuronal health. *Current Topics in Microbiology and Immunology*, *318*, 73–92.

Evangelopoulos, M. E., Koutsis, G., Boufidou, F., & Markianos, M. (2022). Cholesterol levels in plasma and cerebrospinal fluid in patients with clinically isolated syndrome and relapsing-remitting multiple sclerosis. *Neurobiology of Disease*, *174*, 105889.

Fancy, S. P., Kotter, M. R., Harrington, E. P., Huang, J. K., Zhao, C., Rowitch, D. H., & Franklin, R. J. (2010). Overcoming remyelination failure in multiple sclerosis and other myelin disorders. *Experimental Neurology*, *225*, 18–23.

Franklin, R. J. M., & Ffrench-Constant, C. (2017). Regenerating CNS myelin—From mechanisms to experimental medicines. *Nature Reviews Neuroscience*, *18*, 753–769.

Gabrielli, M., Battista, N., Riganti, L., Prada, I., Antonucci, F., Cantone, L., Matteoli, M., Maccarrone, M., & Verderio, C. (2015). Active endocannabinoids are secreted on extracellular membrane vesicles. *EMBO Reports*, *16*, 213–220.

Goldmann, T., Wieghofer, P., Jordão, M. J., Prutek, F., Hagemeyer, N., Frenzel, K., Amann, L., Staszewski, O., Kierdorf, K., Krueger, M., Locatelli, G., Hochgerner, H., Zeiser, R., Epelman, S., Geissmann, F., Priller, J., Rossi, F. M., Bechmann, I., Kerschensteiner, M., … Prinz, M. (2016). Origin, fate and dynamics of macrophages at central nervous system interfaces. *Nature Immunology*, *17*, 797–805.

Goossens, P., Rodriguez-Vita, J., Etzerodt, A., Masse, M., Rastoin, O., Gouirand, V., Ulas, T., Papantonopoulou, O., Van Eck, M., Auphan-Anezin, N., Bebien, M., Verthuy, C., Vu Manh, T. P., Turner, M., Dalod, M., Schultze, J. L., & Lawrence, T. (2019). Membrane cholesterol efflux drives tumor-associated macrophage reprogramming and tumor progression. *Cell Metabolism*, *29*, 1376–1389. e1374.

Grey, M., Dunning, C. J., Gaspar, R., Grey, C., Brundin, P., Sparr, E., & Linse, S. (2015). Acceleration of α-synuclein aggregation by exosomes. *Journal of Biological Chemistry*, *290*, 2969–2982.

Grouleff, J., Irudayam, S. J., Skeby, K. K., & Schiott, B. (2015). The influence of cholesterol on membrane protein structure, function, & dynamics studied by molecular dynamics simulations. *Biochimica Et Biophysica Acta*, *1848*, 1783–1795.

Guo, M., Wang, J., Zhao, Y., Feng, Y., Han, S., Dong, Q., Cui, M., & Tieu, K. (2020). Microglial exosomes facilitate α-synuclein transmission in Parkinson's disease. *Brain*, *143*, 1476–1497.

Hagemeier, K., Brück, W., & Kuhlmann, T. (2012). Multiple sclerosis—Remyelination failure as a cause of disease progression. *Histology and Histopathology*, *27*, 277–287.

Hanafy, K. A., & Sloane, J. A. (2011). Regulation of remyelination in multiple sclerosis. *FEBS Letters*, *585*, 3821–3828.

Herman, S., Djaldetti, R., Mollenhauer, B., & Offen, D. (2022). CSF-derived extracellular vesicles from patients with Parkinson's disease induce symptoms and pathology. *Brain*, *146*(1), 209–224.

Hervera, A., De Virgiliis, F., Palmisano, I., Zhou, L., Tantardini, E., Kong, G., Hutson, T., Danzi, M. C., Perry, R. B., Santos, C. X. C., Kapustin, A. N., Fleck, R. A., Del Río, J. A., Carroll, T., Lemmon, V., Bixby, J. L., Shah, A. M., Fainzilber, M., & Di Giovanni, S. (2018). Reactive oxygen species regulate axonal regeneration through the release of exosomal NADPH oxidase 2 complexes into injured axons. *Nature Cell Biology*, *20*, 307–319.

Hoshino, T., Mahmood, M. I., Mori, K., & Matsuzaki, K. (2013). Binding and aggregation mechanism of amyloid β-peptides onto the GM1 ganglioside-containing lipid membrane. *Journal of Physical Chemistry B*, *117*, 8085–8094.

Hubler, Z., Allimuthu, D., Bederman, I., Elitt, M. S., Madhavan, M., Allan, K. C., Shick, H. E., Garrison, E., Karl, T. M., Factor, D. C., Nevin, Z. S., Sax, J. L., Thompson, M. A., Fedorov, Y., Jin, J., Wilson, W. K., Giera, M., Bracher, F., Miller, R. H., … Adams, D. J. (2018). Accumulation of 8,9-unsaturated sterols drives oligodendrocyte formation and remyelination. *Nature*, *560*, 372–376.

Hussain, R., El-Etr, M., Gaci, O., Rakotomamonjy, J., Macklin, W. B., Kumar, N., Sitruk-Ware, R., Schumacher, M., & Ghoumari, A. M. (2011). Progesterone and Nestorone facilitate axon remyelination: A role for progesterone receptors. *Endocrinology*, *152*, 3820–3831.

Ikeda, K., Yamaguchi, T., Fukunaga, S., Hoshino, M., & Matsuzaki, K. (2011). Mechanism of amyloid β-protein aggregation mediated by GM1 ganglioside clusters. *Biochemistry*, *50*, 6433–6440.

Jiang, H., Zhou, L., Shen, N., Ning, X., Wu, D., Jiang, K., & Huang, X. (2022). M1 macrophage-derived exosomes and their key molecule lncRNA HOTTIP suppress head and neck squamous cell carcinoma progression by upregulating the TLR5/NF-κB pathway. *Cell Death & Disease*, *13*, 183.

Kalluri, R., & LeBleu, V. S. (2020). The biology, function, & biomedical applications of exosomes. *Science*, *367*, eaau6977.

Kotter, M. R., Setzu, A., Sim, F. J., Van Rooijen, N., & Franklin, R. J. (2001). Macrophage depletion impairs oligodendrocyte remyelination following lysolecithin-induced demyelination. *Glia*, *35*, 204–212.

Kotter, M. R., Zhao, C., van Rooijen, N., & Franklin, R. J. (2005). Macrophage-depletion induced impairment of experimental CNS remyelination is associated with a reduced oligodendrocyte progenitor cell response and altered growth factor expression. *Neurobiology of Disease*, *18*, 166–175.

Krämer-Albers, E. M., Bretz, N., Tenzer, S., Winterstein, C., Möbius, W., Berger, H., Nave, K. A., Schild, H., & Trotter, J. (2007). Oligodendrocytes secrete exosomes containing major myelin and stress-protective proteins: Trophic support for axons? *Proteomics - Clinical Applications*, *1*, 1446–1461.

Lau, P., Verrier, J. D., Nielsen, J. A., Johnson, K. R., Notterpek, L., & Hudson, L. D. (2008). Identification of dynamically regulated microRNA and mRNA networks in developing oligodendrocytes. *Journal of Neuroscience*, *28*, 11720–11730.

Lecca, D., Marangon, D., Coppolino, G. T., Méndez, A. M., Finardi, A., Costa, G. D., Martinelli, V., Furlan, R., & Abbracchio, M. P. (2016). MiR-125a-3p timely inhibits oligodendroglial maturation and is pathologically up-regulated in human multiple sclerosis. *Scientific Reports*, *6*, 34503.

Li, C., Qin, T., Liu, Y., Wen, H., Zhao, J., Luo, Z., Peng, W., Lu, H., Duan, C., Cao, Y., & Hu, J. (2021). Microglia-derived exosomal microRNA-151-3p enhances functional healing after spinal cord injury by attenuating neuronal apoptosis via regulating the p53/p21/CDK1 signaling pathway. *Frontiers in Cell and Developmental Biology*, *9*, 783017.

Li, Y., Liu, Z., Song, Y., Pan, J. J., Jiang, Y., Shi, X., Liu, C., Ma, Y., Luo, L., Mamtilahun, M., Shi, Z., Khan, H., Xie, Q., Wang, Y., Tang, Y., Zhang, Z., & Yang, G. Y. (2022). M2 microglia-derived extracellular vesicles promote white matter repair and functional recovery via miR-23a-5p after cerebral ischemia in mice. *Theranostics*, *12*, 3553–3573.

Liu, C., Zhao, Z., Guo, S., Zhang, L., Fan, X., & Zheng, J. (2021). Exosomal miR-27a-3p derived from tumor-associated macrophage suppresses propranolol sensitivity in infantile hemangioma. *Cellular Immunology*, *370*, 104442.

Livesey, M. R., Magnani, D., Cleary, E. M., Vasistha, N. A., James, O. T., Selvaraj, B. T., Burr, K., Story, D., Shaw, C. E., Kind, P. C., Hardingham, G. E., Wyllie, D. J., & Chandran, S. (2016). Maturation and electrophysiological properties of human pluripotent stem cell-derived oligodendrocytes. *Stem Cells*, *34*, 1040–1053.

Lombardi, M., Parolisi, R., Scaroni, F., Bonfanti, E., Gualerzi, A., Gabrielli, M., Kerlero de Rosbo, N., Uccelli, A., Giussani, P., Viani, P., Garlanda, C., Abbracchio, M. P., Chaabane, L., Buffo, A., Fumagalli, M., & Verderio, C. (2019). Detrimental and protective action of microglial extracellular vesicles on myelin lesions: Astrocyte involvement in remyelination failure. *Acta Neuropathologica*, *138*, 987–1012.

Long, R., Gao, L., Li, Y., Li, G., Qin, P., Wei, Z., Li, D., Qian, C., Li, J., & Yang, G. (2021). M2 macrophage-derived exosomes carry miR-1271-5p to alleviate cardiac injury in acute myocardial infarction through down-regulating SOX6. *Molecular Immunology*, *136*, 26–35.

Marschallinger, J., Iram, T., Zardeneta, M., Lee, S. E., Lehallier, B., Haney, M. S., Pluvinage, J. V., Mathur, V., Hahn, O., Morgens, D. W., Kim, J., Tevini, J., Felder, T. K., Wolinski, H., Bertozzi, C. R., Bassik, M. C., Aigner, L., & Wyss-Coray, T. (2020). Lipid-droplet-accumulating microglia represent a dysfunctional and proinflammatory state in the aging brain. *Nature Neuroscience*, *23*, 194–208.

Mathews, E. S., & Appel, B. (2016). Cholesterol biosynthesis supports myelin gene expression and axon ensheathment through modulation of P13K/Akt/mTor signaling. *Journal of Neuroscience*, *36*, 7628–7639.

Mathews, E. S., Mawdsley, D. J., Walker, M., Hines, J. H., Pozzoli, M., & Appel, B. (2014). Mutation of 3-hydroxy-3-methylglutaryl CoA synthase I reveals requirements for isoprenoid and cholesterol synthesis in oligodendrocyte migration arrest, axon wrapping, and myelin gene expression. *Journal of Neuroscience*, *34*, 3402–3412.

McMahon, E. J., Suzuki, K., & Matsushima, G. K. (2002). Peripheral macrophage recruitment in cuprizone-induced CNS demyelination despite an intact blood-brain barrier. *Journal of Neuroimmunology*, *130*, 32–45.

McNamara, N. B., Munro, D. A. D., Bestard-Cuche, N., Uyeda, A., Bogie, J. F. J., Hoffmann, A., Holloway, R. K., Molina-Gonzalez, I., Askew, K. E., Mitchell, S., Mungall, W., Dodds, M., Dittmayer, C., Moss, J., Rose, J., Szymkowiak, S., Amann, L., McColl, B. W., Prinz, M., … Miron, V. E. (2022). Microglia regulate central nervous system myelin growth and integrity. *Nature*, *613*(7942), 120–129.

Meffre, D., Massaad, C., & Grenier, J. (2015). Lithium chloride stimulates PLP and MBP expression in oligodendrocytes via Wnt/β-catenin and Akt/CREB pathways. *Neuroscience*, *284*, 962–971.

Mildner, A., Schmidt, H., Nitsche, M., Merkler, D., Hanisch, U. K., Mack, M., Heikenwalder, M., Brück, W., Priller, J., & Prinz, M. (2007). Microglia in the adult brain arise from Ly-6ChiCCR2+ monocytes only under defined host conditions. *Nature Neuroscience*, *10*, 1544–1553.

Miron, V. E., Boyd, A., Zhao, J. W., Yuen, T. J., Ruckh, J. M., Shadrach, J. L., van Wijngaarden, P., Wagers, A. J., Williams, A., Franklin, R. J. M., & Ffrench-Constant, C. (2013). M2 microglia and macrophages drive oligodendrocyte differentiation during CNS remyelination. *Nature Neuroscience*, *16*, 1211–1218.

Murtie, J. C., Macklin, W. B., & Corfas, G. (2007). Morphometric analysis of oligodendrocytes in the adult mouse frontal cortex. *Journal of Neuroscience Research*, *85*, 2080–2086.

Nelissen, K., Mulder, M., Smets, I., Timmermans, S., Smeets, K., Ameloot, M., & Hendriks, J. J. (2012). Liver X receptors regulate cholesterol homeostasis in oligodendrocytes. *Journal of Neuroscience Research*, *90*, 60–71.

Neumann, B., Segel, M., Chalut, K. J., & Franklin, R. J. (2019). Remyelination and ageing: Reversing the ravages of time. *Multiple Sclerosis*, *25*, 1835–1841.

Nikić, I., Merkler, D., Sorbara, C., Brinkoetter, M., Kreutzfeldt, M., Bareyre, F. M., Brück, W., Bishop, D., Misgeld, T., & Kerschensteiner, M. (2011). A reversible form of axon damage in experimental autoimmune encephalomyelitis and multiple sclerosis. *Nature Medicine*, *17*, 495–499.

Oishi, Y., Spann, N. J., Link, V. M., Muse, E. D., Strid, T., Edillor, C., Kolar, M. J., Matsuzaka, T., Hayakawa, S., Tao, J., Kaikkonen, M. U., Carlin, A. F., Lam, M. T., Manabe, I., Shimano, H., Saghatelian, A., & Glass, C. K. (2017). SREBP1 contributes to resolution of pro-inflammatory TLR4 signaling by reprogramming fatty acid metabolism. *Cell Metabolism*, *25*, 412–427.

Peng, H., Bria, A., Zhou, Z., Iannello, G., & Long, F. (2014). Extensible visualization and analysis for multidimensional images using Vaa3D. *Nature Protocols*, *9*, 193–208.

Raffaele, S., Gelosa, P., Bonfanti, E., Lombardi, M., Castiglioni, L., Cimino, M., Sironi, L., Abbracchio, M. P., Verderio, C., & Fumagalli, M. (2021). Microglial vesicles improve post-stroke recovery by preventing immune cell senescence and favoring oligodendrogenesis. *Molecular Therapy*, *29*, 1439–1458.

Ruckh, J. M., Zhao, J. W., Shadrach, J. L., van Wijngaarden, P., Rao, T. N., Wagers, A. J., & Franklin, R. J. (2012). Rejuvenation of regeneration in the aging central nervous system. *Cell Stem Cell*, *10*, 96–103.

Saher, G., Brugger, B., Lappe-Siefke, C., Mobius, W., Tozawa, R., Wehr, M. C., Wieland, F., Ishibashi, S., & Nave, K. A. (2005). High cholesterol level is essential for myelin membrane growth. *Nature Neuroscience*, *8*, 468–475.

Sariol, A., Mackin, S., Allred, M. G., Ma, C., Zhou, Y., Zhang, Q., Zou, X., Abrahante, J. E., Meyerholz, D. K., & Perlman, S. (2020). Microglia depletion exacerbates demyelination and impairs remyelination in a neurotropic coronavirus infection. *Proceedings of the National Academy of Sciences of the United States of America*, *117*, 24464–24474.

Staugaitis, S. M., Chang, A., & Trapp, B. D. (2012). Cortical pathology in multiple sclerosis: experimental approaches to studies on the mechanisms of demyelination and remyelination. *Acta Neurologica Scandinavica Supplementum*, 97–102.

Takasugi, N., Sasaki, T., Shinohara, M., Iwatsubo, T., & Tomita, T. (2015). Synthetic ceramide analogues increase amyloid-β 42 production by modulating γ-secretase activity. *Biochemical and Biophysical Research Communications*, *457*, 194–199.

Thomas, L. M., & Salter, R. D. (2010). Activation of macrophages by P2×7-induced microvesicles from myeloid cells is mediated by phospholipids and is partially dependent on TLR4. *Journal of Immunology*, *185*, 3740–3749.

Trapp, B. D., Peterson, J., Ransohoff, R. M., Rudick, R., Mörk, S., & Bö, L. (1998). Axonal transection in the lesions of multiple sclerosis. *New England Journal of Medicine*, *338*, 278–285.

Tripathi, A., Volsko, C., Garcia, J. P., Agirre, E., Allan, K. C., Tesar, P. J., Trapp, B. D., Castelo-Branco, G., Sim, F. J., & Dutta, R. (2019). Oligodendrocyte Intrinsic miR-27a Controls Myelination and Remyelination. *Cell Reports*, *29*, 904–919. e909.

Vanherle, S., Haidar, M., Irobi, J., Bogie, J. F. J., & Hendriks, J. J. A. (2020). Extracellular vesicle-associated lipids in central nervous system disorders. *Advanced Drug Delivery Reviews*, *159*, 322–331.

Vanherle, S., Jorissen, W., Dierckx, T., Loix, M., Grajchen, E., Mingneau, F., Guns, J., Gervois, P., Lambrichts, I., Dehairs, J., Swinnen, J. V., Mulder, M. T., Remaley, A. T., Haidar, M., Hendriks, J. J. A., & Bogie, J. J. F. (2022). The ApoA-I mimetic peptide 5A enhances remyelination by promoting clearance and degradation of myelin debris. *Cell Reports*, *41*, 111591.

Voskuhl, R. R., Itoh, N., Tassoni, A., Matsukawa, M. A., Ren, E., Tse, V., Jang, E., Suen, T. T., & Itoh, Y. (2019). Gene expression in oligodendrocytes during remyelination reveals cholesterol homeostasis as a therapeutic target in multiple sclerosis. *Proceedings of the National Academy of Sciences of the United States of America*, *116*, 10130–10139.

Wang, F., Ren, S. Y., Chen, J. F., Liu, K., Li, R. X., Li, Z. F., Hu, B., Niu, J. Q., Xiao, L., Chan, J. R., & Mei, F. (2020). Myelin degeneration and diminished myelin renewal contribute to age-related deficits in memory. *Nature Neuroscience*, *23*, 481–486.

Wang, G., Dinkins, M., He, Q., Zhu, G., Poirier, C., Campbell, A., Mayer-Proschel, M., & Bieberich, E. (2012). Astrocytes secrete exosomes enriched with proapoptotic ceramide and prostate apoptosis response 4 (PAR-4): Potential mechanism of apoptosis induction in Alzheimer disease (AD). *Journal of Biological Chemistry*, *287*, 21384–21395.

Wang, H., Moyano, A. L., Ma, Z., Deng, Y., Lin, Y., Zhao, C., Zhang, L., Jiang, M., He, X., Ma, Z., Lu, F., Xin, M., Zhou, W., Yoon, S. O., Bongarzone, E. R., & Lu, Q. R. (2017). miR-219 cooperates with miR-338 in myelination and promotes myelin repair in the CNS. *Developmental Cell*, *40*, 566–582. e565.

Wang, H., Sui, H., Zheng, Y., Jiang, Y., Shi, Y., Liang, J., & Zhao, L. (2019). Curcumin-primed exosomes potently ameliorate cognitive function in AD mice by inhibiting hyperphosphorylation of the Tau protein through the AKT/GSK-3β pathway. *Nanoscale*, *11*, 7481–7496.

Wang, X., Huang, W., Liu, G., Cai, W., Millard, R. W., Wang, Y., Chang, J., Peng, T., & Fan, G. C. (2014). Cardiomyocytes mediate anti-angiogenesis in type 2 diabetic rats through the exosomal transfer of miR-320 into endothelial cells. *Journal of Molecular and Cellular Cardiology*, *74*, 139–150.

Werkman, I. L., Kövilein, J., de Jonge, J. C., & Baron, W. (2021). Impairing committed cholesterol biosynthesis in white matter astrocytes, but not grey matter astrocytes, enhances in vitro myelination. *Journal of Neurochemistry*, *156*, 624–641.

Witwer, K. W., Goberdhan, D. C., O'Driscoll, L., Théry, C., Welsh, J. A., Blenkiron, C., Buzás, E. I., Di Vizio, D., Erdbrügger, U., Falcón-Pérez, J. M., Fu, Q. L., Hill, A. F., Lenassi, M., Lötvall, J., Nieuwland, R., Ochiya, T., Rome, S., Sahoo, S., & Zheng, L. (2021). Updating MISEV: Evolving the minimal requirements for studies of extracellular vesicles. *Journal of Extracellular Vesicles*, *10*, e12182.

Wolswijk, G. (2002). Oligodendrocyte precursor cells in the demyelinated multiple sclerosis spinal cord. *Brain*, *125*, 338–349.

Woodruff, R. H., Fruttiger, M., Richardson, W. D., & Franklin, R. J. (2004). Platelet-derived growth factor regulates oligodendrocyte progenitor numbers in adult CNS and their response following CNS demyelination. *Molecular and Cellular Neuroscience*, *25*, 252–262.

Xu, P., Xu, H., Tang, X., Xu, L., Wang, Y., Guo, L., Yang, Z., Xing, Y., Wu, Y., Warner, M., Gustafsson, J. A., & Fan, X. (2014). Liver X receptor β is essential for the differentiation of radial glial cells to oligodendrocytes in the dorsal cortex. *Molecular Psychiatry*, *19*, 947–957.

Yuen, T. J., Johnson, K. R., Miron, V. E., Zhao, C., Quandt, J., Harrisingh, M. C., Swire, M., Williams, A., McFarland, H. F., Franklin, R. J., & Ffrench-Constant, C. (2013). Identification of endothelin 2 as an inflammatory factor that promotes central nervous system remyelination. *Brain*, *136*, 1035–1047.

Zhang, C., Li, D., Hu, H., Wang, Z., An, J., Gao, Z., Zhang, K., Mei, X., Wu, C., & Tian, H. (2021). Engineered extracellular vesicles derived from primary M2 macrophages with anti-inflammatory and neuroprotective properties for the treatment of spinal cord injury. *Journal of Nanobiotechnology*, *19*, 373.

Zhao, X., He, X., Han, X., Yu, Y., Ye, F., Chen, Y., Hoang, T., Xu, X., Mi, Q. S., Xin, M., Wang, F., Appel, B., & Lu, Q. R. (2010). MicroRNA-mediated control of oligodendrocyte differentiation. *Neuron*, *65*, 612–626.

SUPPORTING INFORMATION

Additional supporting information can be found online in the Supporting Information section at the end of this article.

How to cite this article: Vanherle, S., Guns, J., Loix, M., Mingneau, F., Dierckx, T., Wouters, F., Kuipers, K., Vangansewinkel, T., Wolfs, E., Lins, P. P., Bronckaers, A., Lambrichts, I., Dehairs, J., Swinnen, J. V., Verberk, S. G. S., Haidar, M., Hendriks, J. J. A., & Bogie, J. F. J. (2023). Extracellular vesicle-associated cholesterol supports the regenerative functions of macrophages in the brain. *Journal of Extracellular Vesicles*, *12,* e12394. https://doi.org/10.1002/jev2.12394